The loss of Ezh2 drives the pathogenesis of myelofibrosis and sensitizes tumor-initiating cells to bromodomain inhibition

Goro Sashida,[1,2]* Changshan Wang,[1,3]* Takahisa Tomioka,[1] Motohiko Oshima,[1] Kazumasa Aoyama,[1] Akinori Kanai,[4] Makiko Mochizuki-Kashio,[1] Hironori Harada,[5] Kazuya Shimoda,[6] and Atsushi Iwama[1]

[1]Department of Cellular and Molecular Medicine, Graduate School of Medicine, Chiba University, Chuo-ku, Chiba 260-8670, Japan
[2]International Research Center for Medical Sciences, Kumamoto University, Chuo-ku, Kumamoto 860-0811, Japan
[3]College of Life Sciences, Inner Mongolia University, Hohhot 010021, China
[4]Department of Molecular Oncology and Leukemia Program Project, Research Institute for Radiation Biology and Medicine, Hiroshima University, Minami-ku, Hiroshima 734-8553, Japan
[5]Department of Hematology, Juntendo University School of Medicine, Bunkyo-ku, Tokyo 113-8421, Japan
[6]Department of Gastroenterology and Hematology, Faculty of Medicine, University of Miyazaki, Miyazaki 889-1692, Japan

EZH2 is a component of polycomb repressive complex 2 (PRC2) and functions as an H3K27 methyltransferase. Loss-of-function mutations in *EZH2* are associated with poorer outcomes in patients with myeloproliferative neoplasms (MPNs), particularly those with primary myelofibrosis (MF [PMF]). To determine how *EZH2* insufficiency is involved in the pathogenesis of PMF, we generated mice compound for an *Ezh2* conditional deletion and activating mutation in *JAK2* (*JAK2V617F*) present in patients with PMF. The deletion of *Ezh2* in *JAK2^V617F* mice markedly promoted the development of MF, indicating a tumor suppressor function for EZH2 in PMF. The loss of Ezh2 in *JAK2^V617F* hematopoietic cells caused significant reductions in H3K27 trimethylation (H3K27me3) levels, resulting in an epigenetic switch to H3K27 acetylation (H3K27ac). These epigenetic switches were closely associated with the activation of PRC2 target genes including *Hmga2*, an oncogene implicated in the pathogenesis of PMF. The treatment of *JAK2^V617F*/*Ezh2*–null mice with a bromodomain inhibitor significantly attenuated H3K27ac levels at the promoter regions of PRC2 targets and down-regulated their expression, leading to the abrogation of MF-initiating cells. Therefore, an EZH2 insufficiency not only cooperated with active JAK2 to induce MF, but also conferred an oncogenic addiction to the H3K27ac modification in MF-initiating cells that was capable of being restored by bromodomain inhibition.

Polycomb-group (PcG) proteins function to maintain gene silencing via histone modifications and are composed of the distinct polycomb repressive complexes (PRCs), PRC1 and PRC2. PRC2 contains EED, SUZ12, and the catalytic component EZH2 or its homologue EZH1, which have been shown to mediate the mono-, di-, and trimethylation of histone H3 at lysine 27 (H3K27me1/me2/me3; Cao et al., 2002). PRC2 components have been characterized as regulators of hematopoietic stem cells (HSCs) as well as oncogenes (Sauvageau and Sauvageau, 2010; Sashida and Iwama, 2012). Although Ezh2 is known to be dispensable for the self-renewal capacity of HSCs (Mochizuki-Kashio et al., 2011; Xie

et al., 2014), it is critical for the propagation of *MLL-AF9*–induced acute myeloid leukemia (AML; Neff et al., 2012; Tanaka et al., 2012), and its overexpression has been shown to induce myeloproliferative neoplasms (MPNs) in mice (Herrera-Merchan et al., 2012). Furthermore, genetic and functional studies identified activating mutations in *EZH2* in malignant B cell lymphomas (Morin et al., 2010; Béguelin et al., 2013), thereby supporting an oncogenic role for EZH2. However, loss-of-function mutations in *EZH2* have also been identified in patients with myelodysplastic syndrome (MDS), MPN, and MDS/MPN diseases, which are clonal myeloid malignancies originating from HSCs (Shih et al., 2012). Loss-of-function mutations in *EZH2* have been shown to predict significantly poorer clinical outcomes in patients with MDS and MPN (Bejar et al., 2011; Guglielmelli et al., 2011). *EZH2* is located at chromosome 7q36.1 and has recently been identified as one of the responsible genes for the pathogenesis of –7/7q– MDS (Kotini et al., 2015). These genetic and clinical findings imply a tumor suppressor role for EZH2 in myeloid malignancies. We also previously demonstrated that the loss

of *Ezh2* promoted the development of MDS in mice in concert with the loss of *Tet2* or *RUNX1* mutants (Muto et al., 2013; Sashida et al., 2014).

MPNs are clonal hematopoietic malignancies that originate from HSCs and are characterized by the excess production of mature myeloid cells and active extramedullary hematopoiesis (EMH) such as in the spleen and liver (Tefferi, 2005). The identification of a somatic activating mutation in JAK2 (JAK2^{V617F}) in patients with MPN, including those with polycythemia vera (PV), essential thrombocytosis (ET), and primary myelofibrosis (MF [PMF]), underlined the importance of the constitutive activation of the JAK–STAT signaling pathway in MPN pathogenesis (Baxter et al., 2005; Kralovics et al., 2005; Levine et al., 2007). Several genetic studies using mouse models including our JAK2^{V617F} transgenic mice showed that the JAK2^{V617F} mutant impaired the self-renewal capacity of HSCs accompanied by enhanced apoptosis and a reduced proliferative capacity (Mullally et al., 2010; Lundberg et al., 2014; Kameda et al., 2015). These findings support JAK2^{V617F} HSCs requiring additional genetic mutations that augment the proliferative capacity of JAK2^{V617F} HSCs. Correspondingly, although most patients with PMF harbor mutations in the JAK–STAT signaling pathway including JAK2^{V617F}, recent genome sequencing experiments revealed concurrent somatic mutations in epigenetic regulators such as *TET2*, *ASXL1*, and *EZH2* (Shih et al., 2012). Of these genes, the loss of *Tet2* has been shown to rescue the impaired function of JAK2^{V617F} HSCs and augment their MPN-initiating capacity (Chen et al., 2015; Kameda et al., 2015), indicating that concurrent gene mutations are critical for the initiation and maintenance of JAK2^{V617F}-induced MPNs.

We previously examined the impact of the hematopoietic cell–specific deletion of *Ezh2* on hematopoiesis. In addition to myelodysplastic features, the loss of *Ezh2* induced increases in platelet counts accompanied by EMH and myeloid-biased hematopoiesis, reminiscent of the clinical phenotypes of patients with MPN (Mochizuki-Kashio et al., 2011; Muto et al., 2013). Loss-of-function mutations in *EZH2* have been detected in ∼10% of patients with MPN including PMF, and half of PMF patients with *EZH2* mutations harbor the *JAK2^{V617F}* mutation (Guglielmelli et al., 2011; Nangalia et al., 2013). A previous study demonstrated that Ezh2 mutations were independently associated with shorter survival in patients with PMF (Guglielmelli et al., 2011). However, the role of EZH2 or PRC2 in the pathogenesis of PMF currently remains unclear. The PRC2 components *SUZ12* and *EED* were recently shown to be frequently deleted or mutated in malignant peripheral nerve sheath tumors (MPNSTs; De Raedt et al., 2014). The loss of PRC2 is known to potentiate the effects of an *NF1* deletion by amplifying Ras-driven transcription through enhanced H3K27 acetylation (H3K27ac) at transcriptional regulatory regions after the loss of H3K27me3. This epigenetic change has been shown to sensitize MPNST cells to BRD4 inhibitors (De Raedt et al., 2014). BRD4 is a member of the bromodomain and extraterminal (BET) family, the members of which bind to acetylated lysine and facilitate transcription (Filippakopoulos et al., 2010). However, the efficacy of BRD4 inhibition on PRC2-insufficient tumors has not yet been determined in different types of tumors.

In the present study, we found that the loss of Ezh2 markedly facilitated the progression of MF in *JAK2^{V617F}* transgenic mice. We demonstrated the effects of the loss of Ezh2 on *JAK2^{V617F}*-induced MF as well as alterations in H3K27 modifications. We also determined the efficacy of JQ1, an inhibitor of BRD4, against *Ezh2*-deficient MF cells in vivo. The results obtained in the present study underlined the importance of additional genetic mutations cooperating with constitutively activated JAK–STAT signaling in the pathogenesis of PMF and also provided a novel therapeutic rationale to improve the clinical outcomes of PMF.

RESULTS

The loss of Ezh2 severely compromised hematopoiesis in the presence of the JAK2^{V617F} mutant

Because *EZH2* loss-of-function mutations have been detected in 5% of PMF patients with *JAK2^{V617F}* mutation, we attempted to determine whether the loss of Ezh2 promoted JAK2^{V617F} mutant–induced MF in vivo. We generated *JAK2^{V617F};Ezh2$^{flox/flox}$;Cre-ERT2* compound mice by crossing *JAK2^{V617F}* transgenic mice and *Ezh2$^{flox/flox}$;Cre-ERT2* conditional KO mice. To exclude any effects of Ezh2 loss and JAK2^{V617F} on nonhematopoietic cells, we transplanted total BM cells isolated from *Cre-ERT2*, *Ezh2$^{flox/flox}$;Cre-ERT2*, *JAK2^{V617F};Cre-ERT2*, and *JAK2^{V617F};Ezh2$^{flox/flox}$;Cre-ERT2* mice into lethally irradiated CD45.1$^+$ WT recipient mice. We then deleted *Ezh2* by activating Cre recombinase via an intraperitoneal injection of tamoxifen at 4 wk after transplantation (Fig. 1 a). We hereafter referred to the recipient mice reconstituted with *Ezh2$^{wt/wt}$*, *Ezh2$^{\Delta/\Delta}$*, *JAK2^{V617F}*, and *JAK2^{V617F}/Ezh2$^{\Delta/\Delta}$* BM cells as WT, Ezh2$^{\Delta/\Delta}$, JAK2^{V617F}, and JAK2^{V617F}/Ezh2$^{\Delta/\Delta}$ mice. We confirmed the successful abolishment of *Ezh2* transcription in cells lacking *Ezh2* (Fig. 1 b) as well as significant reductions in H3K27me3 levels and modest elevations in H3K27ac levels in Lineage marker–negative (Lin$^-$) c-Kit$^+$ BM progenitor cells lacking Ezh2 (Fig. 1 c).

We then investigated whether the loss of Ezh2 promoted the progression of MF in *JAK2^{V617F}* transgenic mice, which develop lethal MF after a long latency. Consistent with our previous findings (Mochizuki-Kashio et al., 2011; Muto et al., 2013), a complete blood count (CBC) analysis of transplanted mice revealed elevated platelet counts in Ezh2$^{\Delta/\Delta}$ mice. JAK2^{V617F}/Ezh2$^{\Delta/\Delta}$ mice showed leukopenia mainly caused by lymphopenia, severe anemia, and variable values of platelet counts at 2 mo after transplantation (4 wk after the deletion of *Ezh2*; Fig. 1, d and e). Among them, moribund JAK2^{V617F}/Ezh2$^{\Delta/\Delta}$ mice developed lethal pancytopenia (Fig. 1 d). We also noted a significant increase in the numbers of neutrophils and monocytes as well as the appearance of dysplastic red blood cells, characteristic features of PMF, in the peripheral blood (PB) of JAK2^{V617F}/Ezh2$^{\Delta/\Delta}$
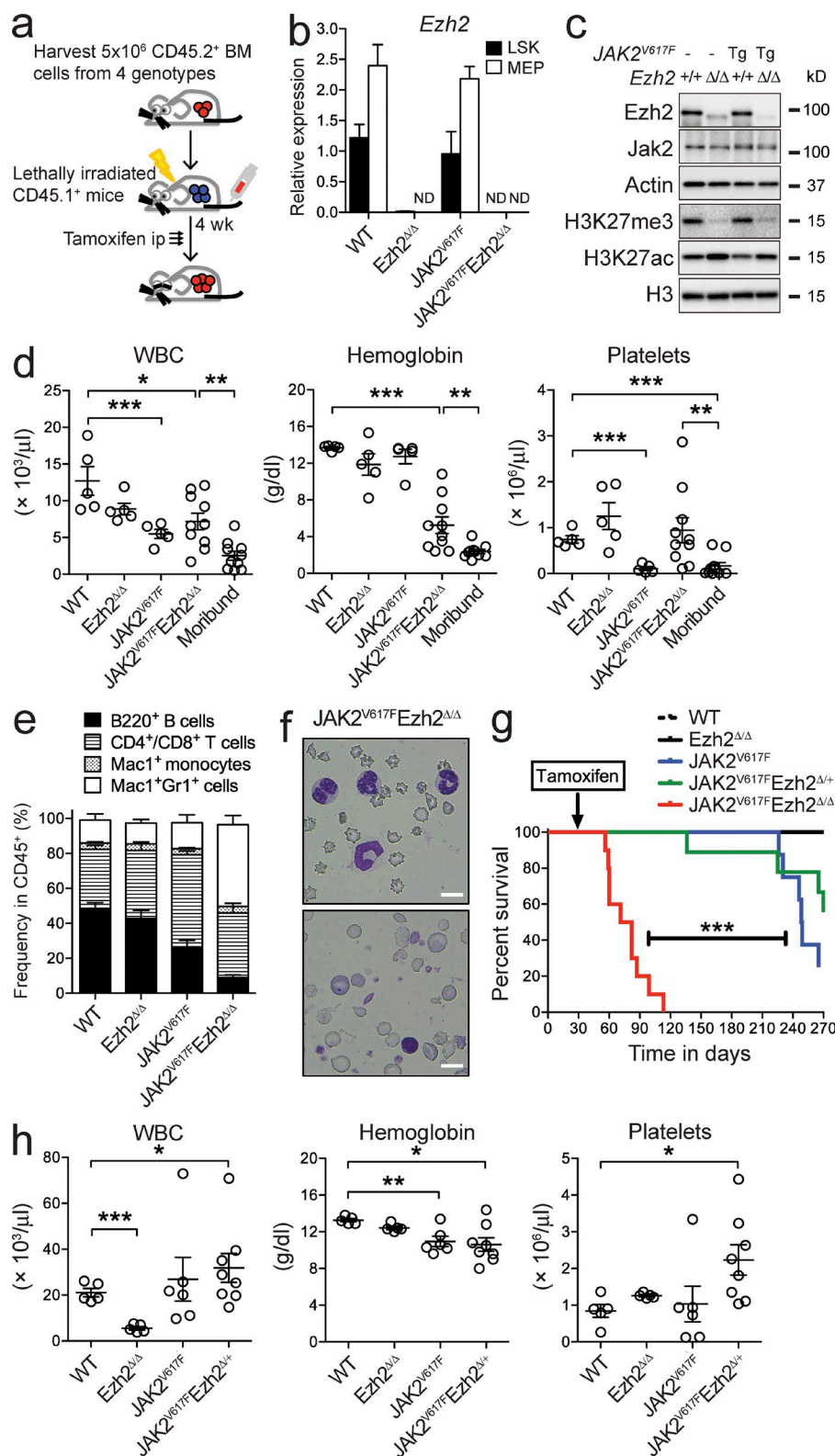
Figure 1. **The loss of Ezh2 severely compromises hematopoiesis in the presence of the JAK2^V617F mutant.** (a) Experimental scheme of our model mouse using *JAK2^V617F* transgenic and *Ezh2* conditional KO BM cells. (b) qRT-PCR analysis of *Ezh2* in LSKs and MEPs from WT, Ezh2^Δ/Δ, JAK2^V617F, and JAK2^V617F/Ezh2^Δ/Δ mice 4 wk after the Cre-mediated deletion of *Ezh2*. (c) Verification of elimination of Ezh2 protein and levels of H3K27me3 in LK cells detected by Western blotting. (d) CBC of WT ($n = 5$), Ezh2^Δ/Δ ($n = 5$), JAK2^V617F ($n = 5$), and JAK2^V617F/Ezh2^Δ/Δ ($n = 10$) mice 4 wk after the deletion of *Ezh2* and moribund JAK2^V617F/Ezh2^Δ/Δ mice ($n = 10$). (e) Proportions of myeloid (Gr-1^+ and/or Mac-1^+), B220^+ B cells, and CD4^+ or CD8^+ T cells among CD45.2^+ donor–derived hematopoietic cells in the PB (JAK2^V617F/Ezh2^Δ/Δ $n = 10$, others $n = 5$). (f) Dysplastic red blood cells in JAK2^V617F/Ezh2^Δ/Δ mice observed by May-Grünewald-Giemsa staining. Bars, 10 µm. (g) Kaplan-Meier survival curves of WT ($n = 6$), Ezh2^Δ/Δ ($n = 6$), JAK2^V617F ($n = 8$), JAK2^V617F/Ezh2^Δ/+ ($n = 9$), and JAK2^V617F/Ezh2^Δ/Δ ($n = 10$) mice; three independent experiments were performed. ***, $P < 0.0001$ by the log-rank test. (h) CBC of WT ($n = 5$), Ezh2^Δ/Δ ($n = 5$), JAK2^V617F ($n = 6$), and JAK2^V617F/Ezh2^Δ/+ ($n = 9$) mice 4 mo after the deletion of *Ezh2*. (a, d, e, and h) Bars and asterisks show the mean ± SEM and *, $P < 0.05$; **, $P < 0.01$; and ***, $P < 0.001$ by the Student's *t* test; two independent experiments. (b and c) Data are shown as mean ± SD; two independent experiments.

mice (Fig. 1 f). As previously reported (Shide et al., 2008), JAK2^V617F mice developed lethal MF after a long latency (median survival 248.5 d), whereas WT and Ezh2^Δ/Δ mice did not develop any lethal hematological malignancies by 9 mo after transplantation (Fig. 1 g). In contrast, JAK2^V617F/Ezh2^Δ/Δ mice readily developed MF-like disease and died by

3 mo after the deletion of *Ezh2* (median survival 76.5 d, P < 0.0001 vs. JAK2^{V617F} mice; Fig. 1 g). Although JAK2^{V617F} mice initially showed severe leukopenia and thrombocytopenia 2 mo after transplantation (Fig. 1 d), gradual increases in white blood cell and platelet counts were observed in the PB and anemia occurred during the development of MF (Fig. 1 h), as previously reported (Shide et al., 2008). Given that *EZH2* haploinsufficiency may contribute to the pathogenesis of myeloid malignancies, we also analyzed JAK2^{V617F}/Ezh2$^{Δ/+}$ mice. Although *Ezh2* heterozygosity in JAK2^{V617F} mice (JAK2^{V617F}/Ezh2$^{Δ/+}$ mice) did not shorten the survival (median survival 280 d, P = 0.552 vs. JAK2^{V617F} mice; Fig. 1 g), it further enhanced leukocytosis and thrombocytosis and promoted anemia (Fig. 1 h). Thus, the loss of Ezh2 severely compromised hematopoiesis and profoundly facilitated the development of a lethal disease in the presence of the JAK2^{V617F} mutant.

The loss of Ezh2 promoted the development of JAK2^{V617F}–induced MF

Because JAK2^{V617F}/Ezh2$^{Δ/Δ}$ mice immediately developed a lethal disease, we next performed detailed phenotypic analyses on the BM and spleen 2 mo after transplantation. JAK2^{V617F}/Ezh2$^{Δ/Δ}$ mice showed significantly reduced BM cell counts with a predominance of mature myeloid cells (Fig. 2, a and b). A histological analysis revealed the presence of dysplastic megakaryocytes accompanied by massive reticular fibers in the BM of JAK2^{V617F}/Ezh2$^{Δ/Δ}$ mice (Fig. 2, c and d). A flow cytometric analysis of the BM showed that the frequency of CD150$^+$CD34$^-$Lin$^-$Sca-1$^+$c-Kit$^+$ (LSK) long-term HSCs (LT-HSCs) was significantly lower in JAK2^{V617F}/Ezh2$^{Δ/Δ}$ mice than in WT mice (Fig. 2 e). In contrast, the frequencies of LSK hematopoietic stem and progenitor cells (HSPCs [LSKs/HSPCs]) and granulocyte/macrophage progenitors (GMPs) in the BM were higher in JAK2^{V617F}/Ezh2$^{Δ/Δ}$ mice than in WT mice (Fig. 2, f and g). Nonetheless, because of the significant reduction in total BM cells, the absolute numbers of LT-HSCs and HSPCs were significantly reduced in JAK2^{V617F}/Ezh2$^{Δ/Δ}$ mice, but those of GMPs were comparable between WT and JAK2^{V617F}/Ezh2$^{Δ/Δ}$ mice (not depicted). Although the frequencies of megakaryocyte/erythroid progenitors (MEPs) were comparable between these genotypes (not depicted), JAK2^{V617F}/Ezh2$^{Δ/Δ}$ mice showed markedly fewer CD71$^+$Ter119$^+$ erythroblasts as the result of enhanced apoptosis, as defined by the greater Annexin V reactivity of CD71$^+$Ter119$^+$ cells in JAK2^{V617F}/Ezh2$^{Δ/Δ}$ mice than either mutation alone (Fig. 2, h and i). Thus, the loss of Ezh2 promoted the commitment of HSCs into myeloid lineages but impaired the production of mature erythroid cells by enhancing apoptosis in the presence of the JAK2^{V617F} mutant.

PMF patients exhibit splenomegaly caused by EMH. As we and other groups have reported (Mullally et al., 2010; Lundberg et al., 2014), JAK2^{V617F} mice and even Ezh2$^{Δ/Δ}$ mice showed myeloproliferative features with splenomegaly and the expansion of myeloid cells in the spleen, and this was more evident in JAK2^{V617F}/Ezh2$^{Δ/Δ}$ mice 4 wk after the dele-

tion of *Ezh2* (Fig. 3, a and b). Hematoxylin and eosin staining of the spleen clearly showed markedly larger red pulp with the greater infiltration of myeloid cells and dysplastic megakaryocytes characterized by hypolobation (Fig. 3 c), as well as the accumulation of more reticular fibers in JAK2^{V617F}/Ezh2$^{Δ/Δ}$ mice than in JAK2^{V617F} mice (Fig. 3 c). Correspondingly, the frequencies of LSKs and Lin$^-$Sca-1$^-$c-Kit$^+$CD150$^+$CD41$^+$ megakaryocyte progenitors (MkPs) were higher in the spleen of JAK2^{V617F} and Ezh2$^{Δ/Δ}$ mice, and this was more prominent in JAK2^{V617F}/Ezh2$^{Δ/Δ}$ mice (Fig. 3 d).

Given that constitutive elevation of thrombopoietin (TPO) was sufficient to develop MF in mice (Kakumitsu et al., 2005), we assessed levels of TPO in the serum and found that JAK2^{V617F}/Ezh2$^{Δ/Δ}$ mice had significantly decreased levels of TPO compared with WT mice (Fig. 4 a). Given that Ezh2 loss enhanced production of IL-6 in an MDS model induced by an oncogenic *RUNX1* mutant (Sashida et al., 2014), we examined expression of inflammatory cytokines and found that the levels of IL-6 and IL-1β were elevated in JAK2^{V617F}/Ezh2$^{Δ/Δ}$ MEPs (Fig. 4 b), which may contribute to the promotion of fibrosis.

We next performed a functional assay to determine whether JAK2^{V617F}/Ezh2$^{Δ/Δ}$ cells were transplantable and developed MF in secondary recipient mice. It has been reported that the spleens of PMF patients contain long-term repopulating HSCs (Wang et al., 2012). We also confirmed that both BM and spleen cells of JAK2^{V617F}/Ezh2$^{Δ/Δ}$ mice developed MF in sublethally irradiated CD45.1$^+$ recipient mice (not depicted). To further assess the repopulating capacity of JAK2^{V617F}/Ezh2$^{Δ/Δ}$ HSPCs, we purified 2,000 LSKs from BM and spleen of WT and JAK2^{V617F}/Ezh2$^{Δ/Δ}$ mice and transplanted them into lethally irradiated mice together with 2×10^5 CD45.1$^+$ WT competitor cells. WT BM LSKs repopulated hematopoiesis better than did WT spleen LSKs in the PB and BM of the recipient mice (Fig. 4, c and d). JAK2^{V617F}/Ezh2$^{Δ/Δ}$ BM and spleen LSKs showed a similar trend, but the difference was mild and not statistically significant (Fig. 4, c and d). These results clearly indicated that the loss of Ezh2 promoted the development of JAK2^{V617F}–induced MF and that MF–initiating cells, which outcompete WT cells in vivo, exist in both BM and spleen in JAK2^{V617F}/Ezh2$^{Δ/Δ}$ mice.

Megakaryocyte–restricted deletion of *Ezh2* contributed to the aggressive phenotype of JAK2^{V617F}–induced MF

The dysplastic megakaryocytes observed in PMF were previously suggested to promote the formation of fibrosis via the excessive production of cytokines and eventually impair hematopoiesis (Tefferi, 2005). Because the loss of Ezh2 combined with the expression of JAK2^{V617F} markedly enhanced the production of dysplastic megakaryocytes in vivo, we determined whether the megakaryocyte-restricted loss of Ezh2 was sufficient to induce MF in the presence of JAK2^{V617F}. To achieve this, we used *Pf4–Cre* transgenic mice, in which Cre-recombinase was driven from the promoter of the *Pf4/Cxcl4* gene specifically expressed in megakaryocyte-com-
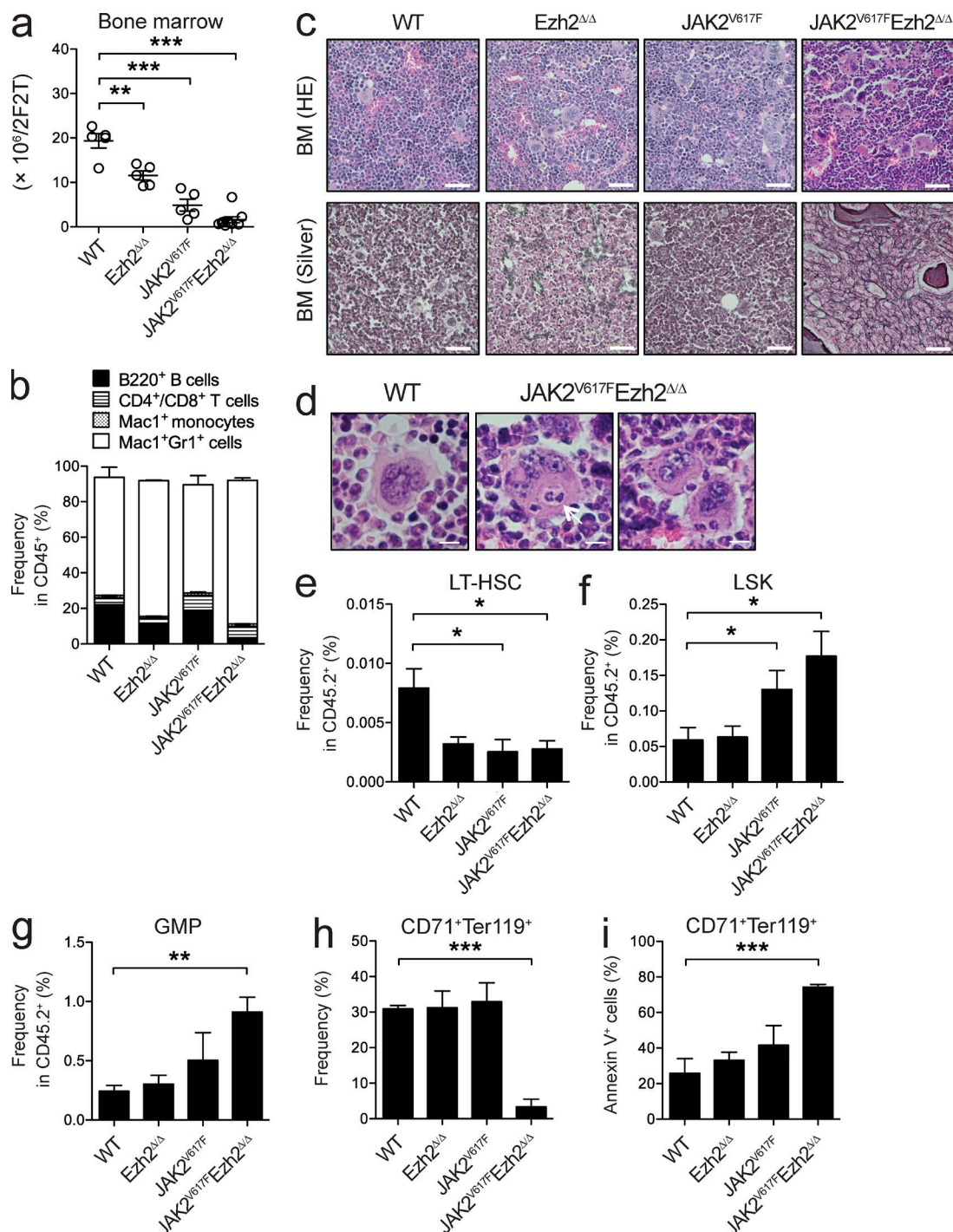
Figure 2. **The loss of Ezh2 promotes the development of JAK2^{V617F}–induced MF.** (a) BM cell counts (two femurs and two tibias) of WT (n = 5), Ezh2$^{\Delta/\Delta}$ (n = 5), JAK2^{V617F} (n = 5), and JAK2^{V617F}/Ezh2$^{\Delta/\Delta}$ (n = 9) mice 4 wk after the deletion of *Ezh2*. (b) Proportions of Gr-1$^+$Mac-1$^+$ neutrophils, Mac-1$^+$ monocytes, B220$^+$ B cells, and CD4$^+$/CD8$^+$ T cells among CD45$^+$ hematopoietic cells in the BM 4 wk after the deletion of *Ezh2*. (c) Histology of the BM from WT, Ezh2$^{\Delta/\Delta}$, JAK2^{V617F}, and JAK2^{V617F}/Ezh2$^{\Delta/\Delta}$ mice observed by hematoxylin-eosin staining (top) and silver staining (bottom). (d) Histology of the BM from WT and JAK2^{V617F}/Ezh2$^{\Delta/\Delta}$ mice observed by hematoxylin-eosin staining (an arrow indicates a megakaryocyte with emperipolesis). (e) Proportions of CD150$^+$CD34$^-$LSK LT-HSCs in the BM of WT, Ezh2$^{\Delta/\Delta}$, JAK2^{V617F}, and JAK2^{V617F}/Ezh2$^{\Delta/\Delta}$ mice (n = 3 each) 4 wk after the deletion of *Ezh2*. (f and g) Proportions of LSKs (f) and GMPs (Lin$^-$Sca-1$^-$c-Kit$^+$CD34$^+$FcγR$^+$; g) in the BM of WT, Ezh2$^{\Delta/\Delta}$, JAK2^{V617F}, and JAK2^{V617F}/Ezh2$^{\Delta/\Delta}$ mice (n = 3 each). (h) Proportions of CD71$^+$Ter119$^+$ double-positive erythroblasts in the BM of WT, Ezh2$^{\Delta/\Delta}$, JAK2^{V617F}, and JAK2^{V617F}/Ezh2$^{\Delta/\Delta}$ mice (n = 5 each) 4 wk after the deletion of *Ezh2*.

mitted progenitors and mature megakaryocytes (Tiedt et al., 2007). We transplanted BM cells from *Pf4-Cre;Ezh2^wt/wt^*, *Pf4-Cre;Ezh2^flox/flox^*, *JAK2^V617F^;Pf4-Cre;Ezh2^wt/wt^*, and *JAK2^V617F^;Pf4-Cre;Ezh2^flox/flox^* mice into lethally irradiated recipients (hereafter referred to as WT, Ezh2$^{Mk\Delta/\Delta}$, JAK2^{V617F}, and JAK2^{V617F}/Ezh2$^{Mk\Delta/\Delta}$, respectively). We confirmed significantly reduced expression of *Ezh2* in MkPs but not in GMPs (Fig. 5 a). A mild reduction in *Ezh2* expression was also observed in LSKs, suggesting leaky expression of Cre in HSPCs, probably in a portion of HSPCs whose cell fate is biased to the megakaryocytic lineage (Yamamoto et al., 2013; Haas et al., 2015). In contrast to the pan-hematopoietic deletion of *Ezh2*, no significant change was observed in platelet counts in Ezh2$^{Mk\Delta/\Delta}$ mice (Fig. 5 b). JAK2^{V617F} and JAK2^{V617F}/Ezh2$^{Mk\Delta/\Delta}$ mice both developed more severe anemia than WT mice 5 mo after transplantation (Fig. 5 b). Although neither JAK2^{V617F} nor Ezh2$^{Mk\Delta/\Delta}$ mice showed splenomegaly, JAK2^{V617F}/Ezh2$^{Mk\Delta/\Delta}$ mice developed severe splenomegaly 5 mo after transplantation (Fig. 5 c). Consistent with EMH in the spleen, the frequencies of LSKs and MkPs in the spleen were higher in JAK2^{V617F}/Ezh2$^{Mk\Delta/\Delta}$ mice than in WT mice (Fig. 5 d). Notably, BM fibrosis and osteosclerosis accompanied with dysplastic megakaryocytes were more prominent in all JAK2^{V617F}/Ezh2$^{Mk\Delta/\Delta}$ mice than in JAK2^{V617F} mice (Fig. 5, e and f). Although 2 out of 12 JAK2^{V617F}/Ezh2$^{Mk\Delta/\Delta}$ mice, but no JAK2^{V617F} mice, developed lethal MF by 6 mo after transplantation, we did not see a significant change in survival outcome between JAK2^{V617F} and JAK2^{V617F}/Ezh2$^{Mk\Delta/\Delta}$ mice during this observation period (median survival undetermined, P = 0.4818). JAK2^{V617F}/Ezh2$^{Mk\Delta/\Delta}$ mice had CD71$^+$Ter119$^+$ cells in the BM at similar frequencies to those of JAK2^{V617F} mice (not depicted), suggesting that the loss of Ezh2 in the erythroid lineage in the presence of JAK2^{V617F} accounted for impaired erythropoiesis. These results indicated that the loss of Ezh2 in *JAK2^V617F^* cells of megakaryocytic lineage largely contributed to the development of aggressive MF observed in JAK2^{V617F}/Ezh2$^{\Delta/\Delta}$ mice.

JAK2^{V617F} and the loss of Ezh2 cooperatively altered transcriptional programs of hematopoiesis

To understand the molecular basis of MPN-initiating cells in JAK2^{V617F}/Ezh2$^{\Delta/\Delta}$ mice, we first performed a gene expression analysis of LSKs and MEPs isolated from the primary recipients 2 mo after transplantation. An integrative analysis identified a set of 1,079 and 1,773 genes that were differentially expressed in JAK2^{V617F}/Ezh2$^{\Delta/\Delta}$ LSKs and MEPs relative to their WT counterparts, respectively (Fig. 6 a). As expected, there was a significant overlap of differentially expressed genes between JAK2^{V617F}, Ezh2$^{\Delta/\Delta}$, and JAK2^{V617F}/Ezh2$^{\Delta/\Delta}$ LSKs and MEPs (Fig. 6 a). However, hierarchical

clustering based on the microarray data of all genes placed JAK2^{V617F}/Ezh2$^{\Delta/\Delta}$ MEPs apart from the other cell populations (Fig. 6 b). Furthermore, a principal component analysis placed JAK2^{V617F} and JAK2^{V617F}/Ezh2$^{\Delta/\Delta}$ LSKs between WT LSKs and WT MEPs, and JAK2^{V617F}/Ezh2$^{\Delta/\Delta}$ MEPs again apart from the others (Fig. 6 c). As the constitutive activation of JAK–STAT5 signaling is critical for the development of MPN, we analyzed the behaviors of target genes in LSKs by using Gene Set Enrichment Analysis (GSEA; Subramanian et al., 2005). We found that STAT5A target genes in human CD34$^+$ HSPCs (Stat5 up-regulated genes) were positively enriched not only in JAK2^{V617F} LSKs, but also in Ezh2$^{\Delta/\Delta}$ LSKs and more significantly enriched in JAK2^{V617F}/Ezh2$^{\Delta/\Delta}$ LSKs than in WT LSKs (Fig. 6 d). Similar results were also observed for Ezh2$^{\Delta/\Delta}$ and JAK2^{V617F}/Ezh2$^{\Delta/\Delta}$ MEPs relative to WT MEPs (not depicted). In addition, we confirmed up-regulation of canonical Stat5 targets such as *Ccl2* and *Il7r* in *Ezh2*-null LSKs by quantitative RT-PCR (qRT-PCR; not depicted). To assess functional activation of Stat5 in these cells, we performed intracellular flow to examine phospho-Stat5 levels. Consistent with the enhanced expression of Stat5-target genes, we observed significant elevation in phospho-Stat5 levels in not only in JAK2^{V617F} LSKs but also Ezh2$^{\Delta/\Delta}$ LSKs in response to IL-3 stimulation (Fig. 6 e), and similar results were observed in Lin$^-$c-Kit$^+$ (LK) myeloid progenitors (not depicted). Notably, JAK2^{V617F}/Ezh2$^{\Delta/\Delta}$ LSKs showed significantly elevated levels of phosho-Stat5 regardless of the IL-3 stimulation (Fig. 6 e), implying that the loss of Ezh2 cooperated with JAK2^{V617F} to induce high basal activation levels of Stat5. This synergistic effect may partly account for the altered gene expression profiles of JAK2^{V617F}/Ezh2$^{\Delta/\Delta}$ LSKs and MEPs and also the promotion of JAK2^{V617F}-induced MF in the absence of Ezh2.

In an attempt to understand changes in the gene expression profile of JAK2^{V617F}/Ezh2$^{\Delta/\Delta}$ HSPCs in more detail, we performed GSEA using a canonical PRC2 target gene set that was defined by the chromatin immunoprecipitation (ChIP)-sequencing (ChIP-seq) of H3K27me3 modification in WT LSK HSPCs (Table S1). The positive enrichment of canonical PRC2 targets was significantly greater in Ezh2$^{\Delta/\Delta}$ LSKs than in WT LSKs, regardless of the presence of JAK2^{V617F} (Fig. 6 f). In contrast, canonical PRC2 targets were negatively enriched in JAK2^{V617F} LSKs (Fig. 6 f).

We next used the gene sets generated from distinct hematopoietic cell fractions in GSEA. As we reported previously, the loss of Ezh2 did not compromise HSC function and the expression of HSC signature genes (Chambers et al., 2007) was largely retained (Fig. 6 g). In contrast, because the JAK2^{V617F} mutant impairs HSC function, as described pre-

(i) Proportions of Annexin V$^+$ apoptotic cells in CD71$^+$Ter119$^+$ erythroblasts in the BM of WT, Ezh2$^{\Delta/\Delta}$, JAK2^{V617F}, and JAK2^{V617F}/Ezh2$^{\Delta/\Delta}$ mice (*n* = 3 each). (a, b, and e–i) Bars and asterisks show the mean ± SEM and *, P < 0.05; **, P < 0.01; and ***, P < 0.001 by the Student's *t* test; two independent experiments. Bars: (c) 50 µm; (d) 10 µm.
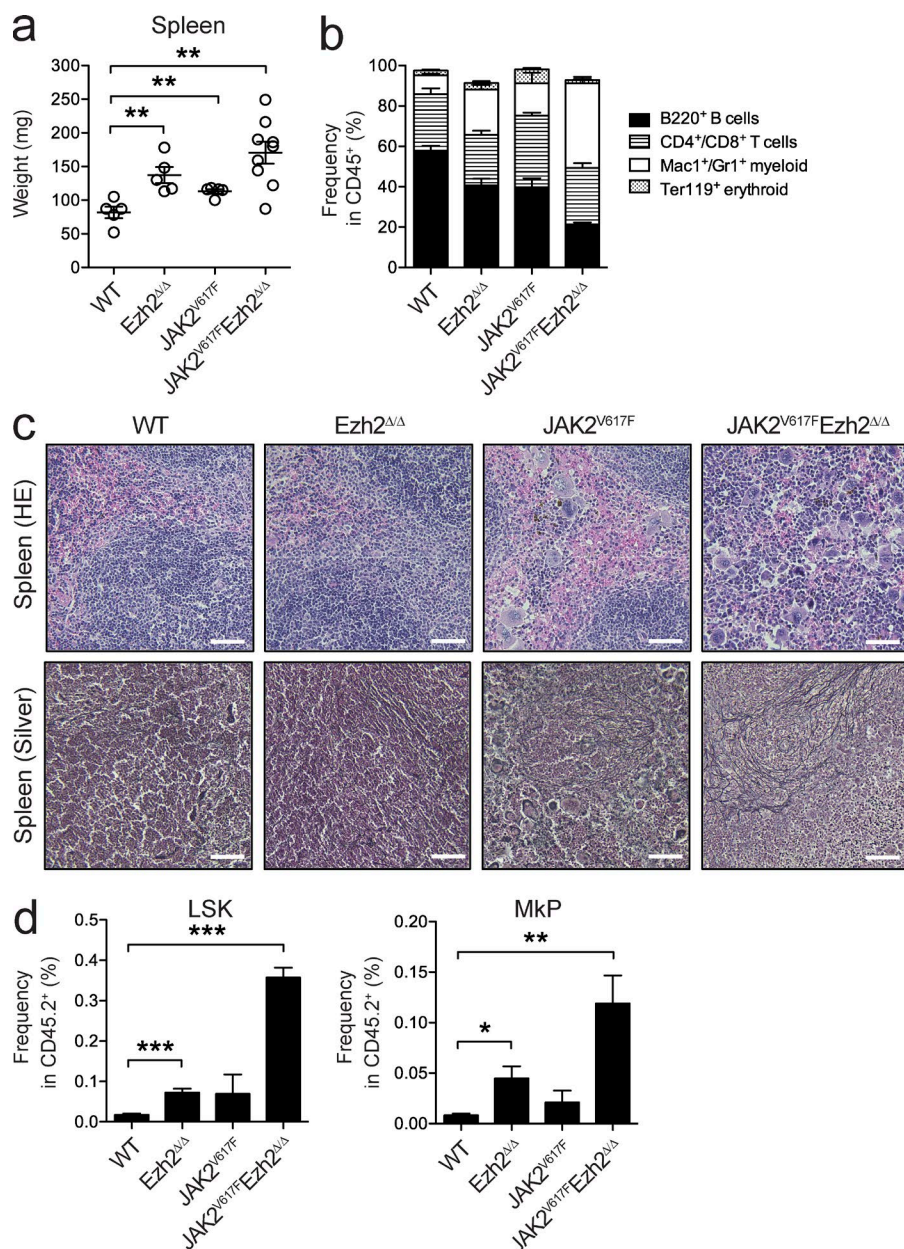
Figure 3. **The loss of Ezh2 promotes the development of EMH.** (a) Spleen weight of WT ($n = 5$), Ezh2$^{\Delta/\Delta}$ ($n = 5$), JAK2^{V617F} ($n = 5$), and JAK2^{V617F}/Ezh2$^{\Delta/\Delta}$ ($n = 9$) mice 4 wk after the deletion of *Ezh2*. (b) Proportions of Gr-1$^+$ and/or Mac-1$^+$ myeloid, B220$^+$ B cells, CD4$^+$ or CD8$^+$ T cells, and Ter119$^+$ erythroid cells among CD45$^+$ hematopoietic cells in the spleen. (c) Histology of the spleen from WT, Ezh2$^{\Delta/\Delta}$, JAK2^{V617F}, and JAK2^{V617F}/Ezh2$^{\Delta/\Delta}$ mice observed by hematoxylin-eosin staining (top) and silver staining (bottom). Bars, 50 µm. (d) Proportions of LSKs and MkPs (Lin$^-$Sca-1$^-$c-Kit$^+$C-D150$^+$CD41$^+$) in the spleen of WT, Ezh2$^{\Delta/\Delta}$, JAK2^{V617F}, and JAK2^{V617F}/Ezh2$^{\Delta/\Delta}$ mice ($n = 5$–9) 4 wk after the deletion of *Ezh2*. (a, b, and d) Bars and asterisks show the mean ± SEM and *, $P < 0.05$; **, $P < 0.01$; and ***, $P < 0.001$ by the Student's *t* test; two independent experiments.

viously (Kameda et al., 2015), the expression of HSC signature genes was significantly compromised in JAK2^{V617F} LSKs (Fig. 6 g). Correspondingly, the negative enrichment of HSC signature genes was greater in JAK2^{V617F}/Ezh2$^{\Delta/\Delta}$ mice than in WT mice but was lower than that in JAK2^{V617F} mice (Fig. 6, g and h), implying that the loss of Ezh2 partly restored the impaired function of JAK2^{V617F} HSCs. Furthermore, as indicated by the principal component analysis (Fig. 6 c), the gene set of MkPs (Pronk et al., 2007) was positively enriched in JAK2^{V617F}/Ezh2$^{\Delta/\Delta}$ LSKs only (Fig. 6 g). These results indicated that JAK2^{V617F} and the loss of Ezh2 cooperated to activate the transcriptional program driving megakaryopoiesis in HSPCs.

Alteration in H3K27me3 upon the loss of Ezh2 resulted in the activation of specific oncogenes

We performed ChIP-seq of H3K27me3 in purified LSKs isolated from WT and JAK2^{V617F}/Ezh2$^{\Delta/\Delta}$ mice 1–2 mo after the deletion of *Ezh2* to understand how epigenetic modifications were altered to reprogram transcriptional profiles in HSPCs upon the induction of JAK2^{V617F} followed by the loss of Ezh2. We first assessed H3K27me3 levels at promoter regions between 2.0 kb upstream and downstream of the transcription start sites (TSSs) of RefSeq genes. As expected, the level of H3K27me3 in JAK2^{V617F}/Ezh2$^{\Delta/\Delta}$ LSK cells was significantly lower than that in WT LSKs (Fig. 7 a), and 2,073 genes showed lower levels of H3K27me3 in JAK2^{V617F}/
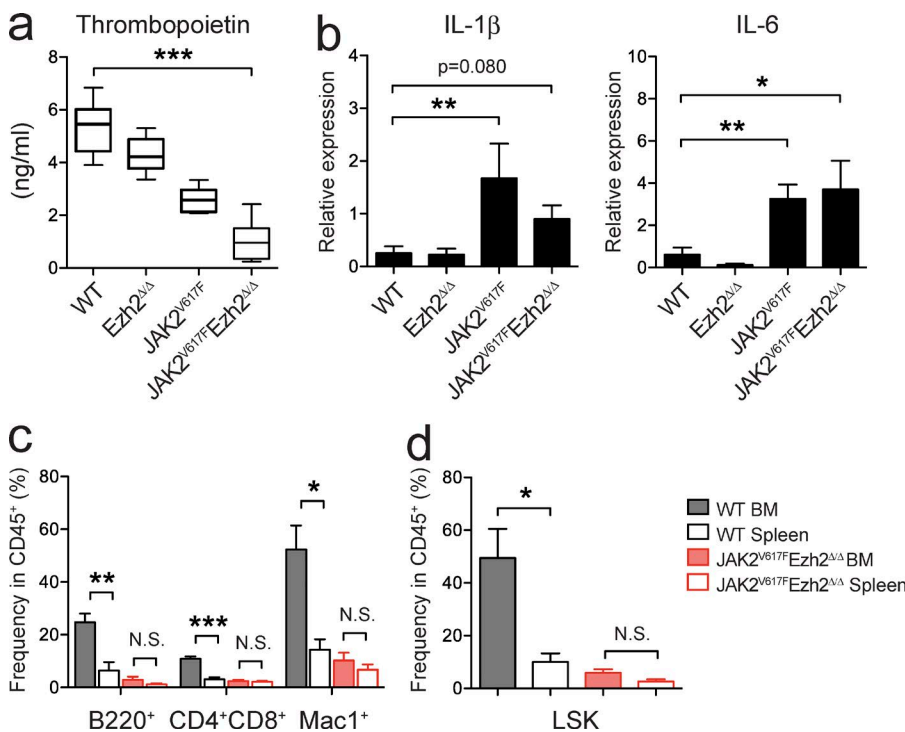
Figure 4. MF-initiating cells are present in the BM and spleen of JAK2^{V617F}/Ezh2$^{\Delta/\Delta}$ mice. (a) Levels of TPO protein in the serum of WT ($n = 6$), Ezh2$^{\Delta/\Delta}$ ($n = 4$), JAK2^{V617F} ($n = 4$), and JAK2^{V617F}/Ezh2$^{\Delta/\Delta}$ ($n = 4$) mice 1–2 mo after the deletion of *Ezh2*. (b) qRT-PCR analysis of *Il6* and *Il1β* in MEPs from WT ($n = 6$), Ezh2$^{\Delta/\Delta}$ ($n = 8$), JAK2^{V617F} ($n = 8$), and JAK2^{V617F}/Ezh2$^{\Delta/\Delta}$ ($n = 8$) mice 1–2 mo after the deletion of *Ezh2*. (c and d) Chimerism of CD45.2$^+$ donor cells in Mac1$^+$ myeloid cells, B220$^+$ B cells, and CD4$^+$/CD8$^+$ T cells in the PB (c) and BM LSK cells (d) of CD45.1$^+$ recipients ($n = 5$ each) at 3 mo after transplantation of BM and spleen LSKs isolated from WT and JAK2^{V617F}/Ezh2$^{\Delta/\Delta}$ mice. (a–d) Bars and asterisks show the mean ± SEM and *, P < 0.05; **, P < 0.01; and ***, P < 0.001 by the Student's *t* test; two independent experiments.

Ezh2$^{\Delta/\Delta}$ LSKs than in WT LSKs (Fig. 7 b). Furthermore, the genes in the MkP gene set, which was positively enriched in JAK2^{V617F}/Ezh2$^{\Delta/\Delta}$ LSK cells (Fig. 6 g), led to significantly lower H3K27me3 levels in JAK2^{V617F}/Ezh2$^{\Delta/\Delta}$ LSK cells than in WT LSK cells (Fig. 7 c), suggesting that the majority of megakaryocytic genes were transcriptionally repressed by Ezh2 in LSK HSPCs.

We then attempted to determine how the loss of Ezh2 impacted oncogene expression associated with the propagation of MF. Among 2,073 genes losing H3K27me3 in JAK2^{V617F}/Ezh2$^{\Delta/\Delta}$ LSKs (Fig. 7 b), we found that 243 genes were highly derepressed, which included several potential oncogenes such as *Hmga2*, *Mlf1*, and *Pbx3* (Fig. 7 d and Table S2) in a manner similar to our previous observation in Tet2$^{KD/KD}$Ezh2$^{\Delta/\Delta}$ MDS cells (Muto et al., 2013). The expression of *Hmga2* was significantly elevated upon the loss of Ezh2 in LSKs and MEPs regardless of the presence of JAK2^{V617F}, and its activation was more evident in MEPs, in which *Hmag2* physiologically undergoes transcriptional repression (Fig. 7, e and f). The transduction of Hmga2 in WT HSCs has been shown to promote megakaryopoiesis (Oguro et al., 2012); therefore, we examined the effects of the ectopic expression of *Hmga2* in combination with JAK2^{V617F} on the production of megakaryocytes. The transduction of *Hmga2* in WT HSCs promoted the cell growth and increased the frequencies of megakaryocytes in culture in the presence of SCF and TPO (Fig. 7, g–i). In contrast, overexpression of *Hmga2* in JAK2^{V617F} HSCs, which showed limited proliferation in culture, did not enhance cell growth (Fig. 7 g). Instead, it markedly promoted the megakaryocytic differentiation of *JAK2^{V617F}* HSCs and

induced dysplastic megakaryocytes characterized by loose lobulation and various size (Fig. 7, h and i). These findings implicate the derepressed *Hmga2* in the expansion of abnormal megakaryocytes in JAK2^{V617F}/Ezh2$^{\Delta/\Delta}$ mice. This result appeared to be relevant to the activation of *HMGA2* in CD34$^+$ HSPCs in patients with PMF (Guglielmelli et al., 2007; Harada–Shirado et al., 2015). Collectively, these results demonstrated that the loss of Ezh2 in the presence of the JAK2^{V617F} mutant reduced H3K27me3 levels and induced the activation of oncogenic Ezh2 targets such as *Hmga2*.

Inhibition of BRD4 abrogated the MF–initiating capacity of JAK2^{V617F}/Ezh2–null cells

The loss of SUZ12 has been shown to promote the consequential gain of H3K27ac after the loss of H3K27me3 in MPNST cells (De Raedt et al., 2014). In the present study, we also noted a global elevation in H3K27ac in Ezh2–null hematopoietic cells (Fig. 1 c). To understand how the altered H3K27me3 modification at transcriptional regulatory regions facilitated the pathogenesis of MF, we investigated whether JQ1, a Brd4 inhibitor (Filippakopoulos et al., 2010), perturbed the development of MF in JAK2^{V617F}/Ezh2$^{\Delta/\Delta}$ mice. First, to determine whether there is a therapeutic specificity of JQ1 to mutant cells, we generated chimeric mice engrafted with CD45.1$^+$ WT cells and CD45.2$^+$ mutant cells and treated them with JQ1 (45 g/kg/day) every other day for 2 wk (Fig. 8 a). Notably, mutant cells were more susceptible to JQ1 treatment compared with coexisting WT cells, and among mutants, JAK2^{V617F}/Ezh2$^{\Delta/\Delta}$ cells showed the best response to JQ1 (Fig. 8 b), suggesting that there is a
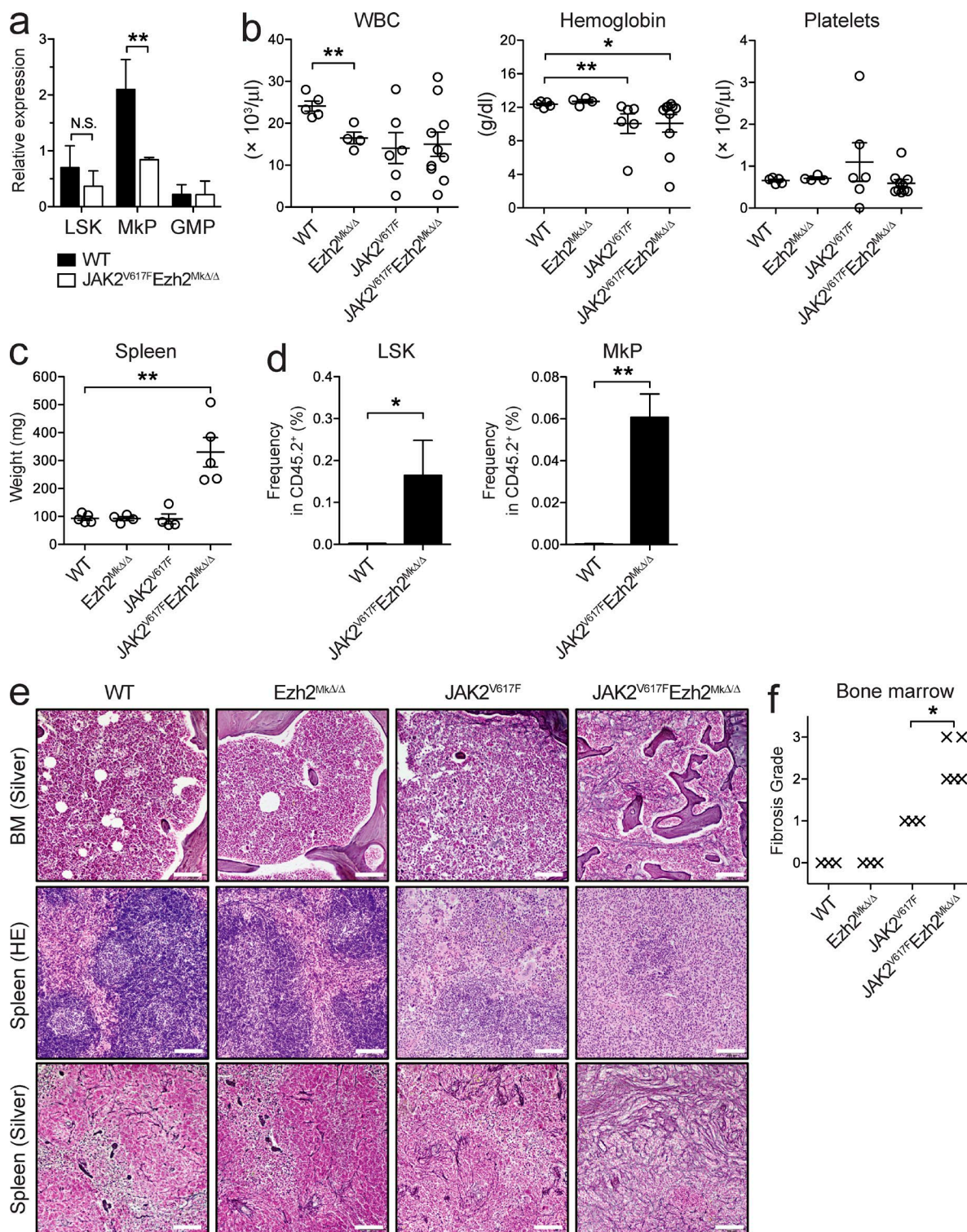
Figure 5. **Megakaryocyte–restricted deletion of *Ezh2* contributes to the progression of JAK2^{V617F}–induced fibrosis.** (a) qRT-PCR analysis of *Ezh2* in LSKs, MkPs, and GMPs from WT and JAK2^{V617F}/Ezh2$^{MkΔ/Δ}$ cells at 2–3 mo after transplantation. (b) CBC of WT ($n = 5$), Ezh2$^{MkΔ/Δ}$ ($n = 4$), JAK2^{V617F} ($n = 6$), and JAK2^{V617F}/Ezh2$^{MkΔ/Δ}$ ($n = 10$) mice 5 mo after transplantation. (c) Spleen weight of WT ($n = 5$), Ezh2$^{MkΔ/Δ}$ ($n = 4$), JAK2^{V617F} ($n = 4$), and JAK2^{V617F}/Ezh2$^{MkΔ/Δ}$ ($n = 5$) mice 5 mo after transplantation. (d) Proportions of LSK cells and MkPs in the spleen of WT and JAK2^{V617F}/Ezh2$^{MkΔ/Δ}$ mice ($n = 3–5$) 5 mo after trans-plantation. (e) Histology of the BM and spleen from WT, Ezh2$^{MkΔ/Δ}$, JAK2^{V617F}, and JAK2^{V617F}/Ezh2$^{MkΔ/Δ}$ mice observed by hematoxylin-eosin staining (middle)

therapeutic window of JQ between WT and mutant cells in vivo. Furthermore, to determine whether JQ1 could abrogate MF–initiating cells, we administered either control DMSO or JQ1 (45 mg/kg/day) to WT mice and JAK2^{V617F}/Ezh2$^{\Delta/\Delta}$ mice intraperitoneally every other day for 2 wk (Fig. 8 c). No significant differences were observed in hemoglobin levels between JQ1-treated WT mice and control WT mice; however, JAK2^{V617F}/Ezh2$^{\Delta/\Delta}$ mice showed advanced anemia after the JQ1 treatment (Fig. 8 d). The JQ1 treatment did not significantly prolong the survival of JAK2^{V617F}/Ezh2$^{\Delta/\Delta}$ mice over nontreated mice, possibly because of severe anemia after the JQ1 treatment (85 d vs. 75.5 d, P = 0.088, n = 6 each). However, advanced fibrosis in the BM was more attenuated in JQ1-treated JAK2^{V617F}/Ezh2$^{\Delta/\Delta}$ mice than in nontreated JAK2^{V617F}/Ezh2$^{\Delta/\Delta}$ mice (Fig. 8 e). Spleen size was significantly smaller in JQ1-treated JAK2^{V617F}/Ezh2$^{\Delta/\Delta}$ mice than in nontreated JAK2^{V617F}/Ezh2$^{\Delta/\Delta}$ mice at 4 wk after treatment (Fig. 8 f), indicating that JQ1 profoundly suppressed EMH in JAK2^{V617F}/Ezh2$^{\Delta/\Delta}$ mice. Nevertheless, LSK cells and MkPs remained in the spleen of JQ1-treated JAK2^{V617F}/Ezh2$^{\Delta/\Delta}$ mice at similar frequencies to those of nontreated JAK2^{V617F}/Ezh2$^{\Delta/\Delta}$ mice (Fig. 8 g). To evaluate the effects of JQ1 on MF–initiating cells in JAK2^{V617F}/Ezh2$^{\Delta/\Delta}$ mice, we transplanted 10^6 spleen cells isolated from JQ1 or DMSO-treated WT mice and JAK2^{V617F}/Ezh2$^{\Delta/\Delta}$ mice into sublethally irradiated CD45.1$^+$ recipient mice (Fig. 8 c). JQ1 treatment did not compromise the repopulating capacity of WT spleen cells, which contributed to the PB cells as well as LSKs in the BM and spleen of the recipient mice at comparable levels with DMSO-treated cells (Fig. 8, h and i). In contrast, JQ1-treated JAK2^{V617F}/Ezh2$^{\Delta/\Delta}$ cells barely contributed to the repopulation of recipient hematopoiesis, particularly Mac1$^+$ myeloid cells in the PB cells and LSKs in the BM and spleen of the recipient mice, whereas DMSO-treated JAK2^{V617F}/Ezh2$^{\Delta/\Delta}$ cells established significant levels of repopulation (Fig. 8, h and i). These results indicated that the administration of JQ1 abrogated MF–initiating cells in JAK2^{V617F}/Ezh2$^{\Delta/\Delta}$ mice.

To understand how JQ1 altered H3K27ac modifications in the absence of Ezh2 and impaired MF–initiating capacity, we performed ChIP-seq for H3K27ac using purified LK cells because of the paucity of cells recovered after the JQ1 treatment. Although JQ1-treated JAK2^{V617F}/Ezh2$^{\Delta/\Delta}$ cells showed significant but mild elevation in H3K27ac levels at the enhancer regions defined in HSPCs (Lara-Astiaso et al., 2014) relative to the nontreated cells (Fig. 9 a), H3K27ac levels at the promoter regions were significantly lower in JQ1-treated cells than in the nontreated cells (Fig. 9 a). A set of 7,827 genes showed reduced H3K27ac levels at the promoter regions that were more than twofold lower in JQ1-treated LK cells than in nontreated LK cells (Fig. 9 b) and thus were defined as JQ1 targets (Table S1).

These results indicated that JQ1 markedly decreased H3K27ac levels at the promoter regions, at least in this context.

We next performed GSEA in LSK cells isolated from JAK2^{V617F}/Ezh2$^{\Delta/\Delta}$ mice immediately after completion of the JQ1 treatment. Although BRD4 inhibition has been reported to repress c-Myc–dependent transcription in specific types of tumors including AML cells (Dawson et al., 2011), c-Myc targets did not show significant negative enrichment in JQ1-treated LSKs relative to DMSO-treated LSKs (not depicted), implying that BRD4 inhibition suppressed disease-initiating cells in a c-Myc–independent manner. As reported in MPN ST cells, GSEA clearly revealed the greater transcriptional repression of PRC2 target genes in JQ1-treated LSKs than in nontreated LSKs (Fig. 9 c), indicating that H3K27ac-mediated transcriptional activation was largely responsible for the activation of PRC2 target genes in this context. Indeed, JQ1 targets, which lost H3K27ac levels more than twofold in JQ1-treated LK cells, were overlapped with most of the canonical PRC2 target genes (Fig. 9 d). Correspondingly, JQ1-treated cells showed significantly lower levels of H3K27ac at the promoter regions of PRC2 targets in LK cells than nontreated LK cells (Fig. 9 e). Given the importance of Hmga2 in the pathogenesis of MF, we next focused on the *Hmga2* locus and confirmed significant reductions in H3K27ac levels at the promoter regions in JQ1-treated JAK2^{V617F}/Ezh2$^{\Delta/\Delta}$ LK cells (Fig. 9 f). Consistent with the reduction observed in H3K27ac levels, the expression of *Hmga2* was specifically lower in JQ-treated MEPs, which reside in the LK fraction but not in LSK cells, than that in DMSO-treated cells (Fig. 9 g). The administration of JQ1 did not repress the expression of *Hmga2* in either of the WT cells (Fig. 9 g). GSEA also showed that the MkP gene set became negatively enriched in JAK2^{V617F}/Ezh2$^{\Delta/\Delta}$ LSKs upon the JQ1 treatment relative to that in DMSO-treated cells (Fig. 9 h). Functional annotation based on Gene Ontology (GO) biological processes showed that the enrichment of genes that fell into categories such as cell cycle, RNA processing, translation, and DNA damage repair was significantly greater in JQ1-treated cells than in the nontreated cells (Fig. 9 i). Collectively, the activation of genes in these biological processes together with down-regulation of oncogenic Ezh2 target genes may have abrogated the MF–initiating capacity of JAK2^{V617F}/Ezh2$^{\Delta/\Delta}$ cells after the JQ1 treatment.

DISCUSSION

In the present study, we demonstrated that the deletion of *Ezh2*, a frequently mutated gene in MPN patients, promoted the development of *JAK2^{V617F}*-induced MF in vivo. MPN is now recognized as a disorder with augmented intracellular signaling because the majority of patients harbor activating mutations in genes regulating JAK–STAT signaling (e.g.,

---

and silver staining (top and bottom). Bars, 100 µm. (f) BM fibrosis grading (grades 0–3; Thiele et al., 2005) of WT, Ezh2$^{Mk\Delta/\Delta}$, JAK2^{V617F}, and JAK2^{V617F}/Ezh2$^{Mk\Delta/\Delta}$ (n = 3–5) mice 5 mo after transplantation. (a–d) Bars and asterisks show the mean ± SEM and *, P < 0.05; and **, P < 0.01 by the Student's t test. (f) Asterisk shows *, P < 0.05 by the Mann–Whitney U test; two independent experiments.
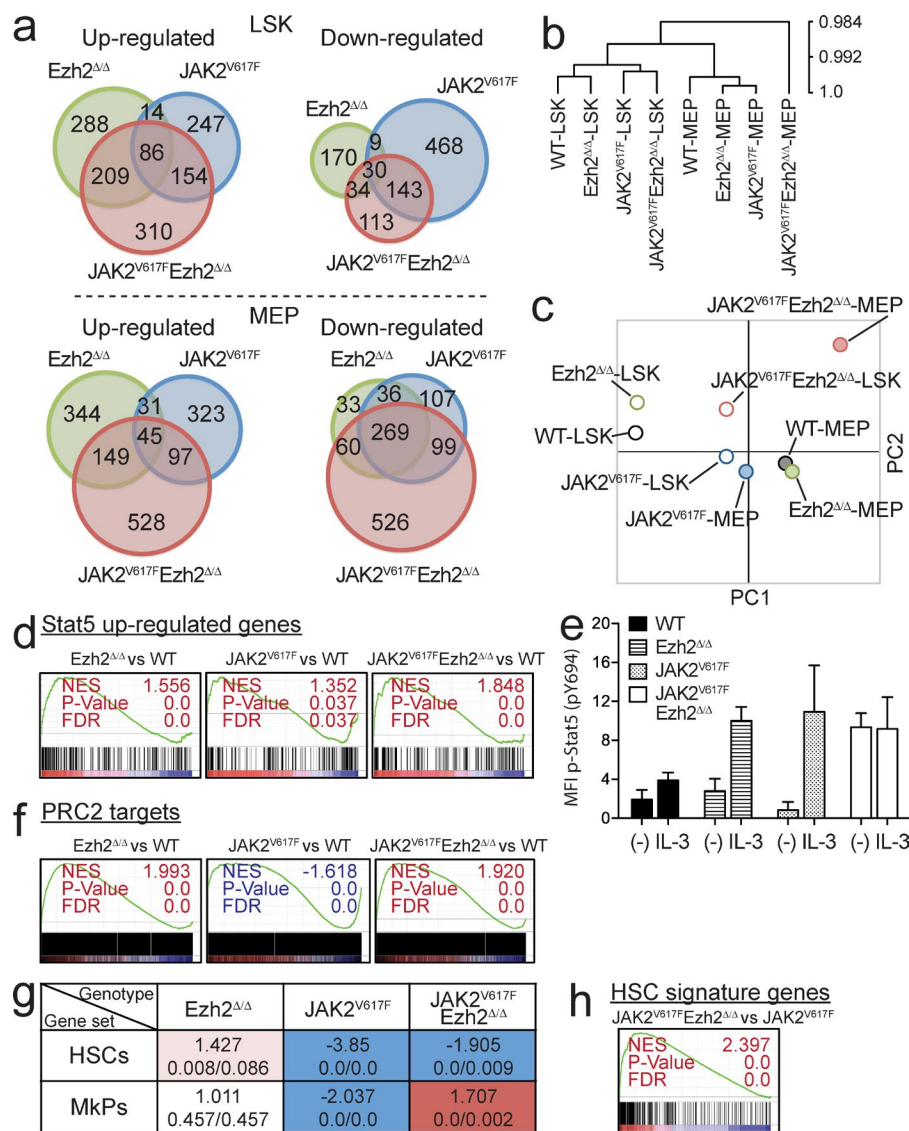
Figure 6. **JAK2^V617F and the loss of Ezh2 cooperatively alter transcriptional programs of hematopoiesis.** (a) Venn diagrams showing overlaps of up- and down-regulated genes (left and right, respectively) between Ezh2^Δ/Δ, JAK2^V617F, and JAK2^V617F/Ezh2^Δ/Δ LSKs and MEPs isolated 4 wk after the deletion of *Ezh2* relative to their WT counterparts. (b) Hierarchical clustering based on total gene expression in LSKs and MEPs isolated from WT, Ezh2^Δ/Δ, JAK2^V617F, and JAK2^V617F/Ezh2^Δ/Δ mice (linkage scores are indicated on the right). (c) A principal component (PC) analysis based on total gene expression in LSKs (open circles) and MEPs (closed circles) isolated from WT, Ezh2^Δ/Δ, JAK2^V617F, and JAK2^V617F/Ezh2^Δ/Δ mice. (d) GSEA plots for Stat5 up-regulated genes defined in human HSPCs comparing mouse LSKs isolated from WT, Ezh2^Δ/Δ, JAK2^V617F, and JAK2^V617F/Ezh2^Δ/Δ mice. (e) Levels of the mean fluorescence intensity (MFI) of phospho-Stat5 (p-Y694) in LSKs from WT, Ezh2^Δ/Δ, JAK2^V617F, and JAK2^V617F/Ezh2^Δ/Δ (*n* = 3 each) mice after serum starvation ("(−)") and stimulation of IL-3 ("IL-3"). Bars show the mean ± SEM; three independent experiments. (f) GSEA plots for canonical PRC2 targets defined in LSK HSPCs comparing LSKs isolated from WT, Ezh2^Δ/Δ, JAK2^V617F, and JAK2^V617F/Ezh2^Δ/Δ mice. (g) GSEA for gene expression signatures of HSCs and MkPs comparing LSKs isolated from WT, Ezh2^Δ/Δ, JAK2^V617F, and JAK2^V617F/Ezh2^Δ/Δ mice (the NES, p-value, and FDR q-value [top and bottom rows, respectively] relative to WT LSKs are shown in each cell). (h) GSEA plots for the HSC signature in LSKs isolated from JAK2^V617F/Ezh2^Δ/Δ compared with JAK2^V617F mice. (a–d and f–h) Experiments used cells from two to four mice individual mice per genotype. (d and f–h) The normalized enrichment score (NES), nominal p-value, and false discovery rate (FDR) q-value are indicated.

JAK2 or *c-MPL*) or *CALR* (Klampfl et al., 2013; Nangalia et al., 2013). However, recent genome-wide sequencing studies revealed frequent co-occurring mutations in epigenetic regulators such as *TET2*, *ASXL1*, and *EZH2* (Shih et al., 2012). Loss-of-function mutations in *EZH2* have been identified in ~10% of patients with PMF (Guglielmelli et al., 2011). We previously reported that *Ezh2*-deficient mice showed MPN-like phenotypes, such as increased platelet counts with EMH and myeloid-biased hematopoiesis at the expense of lymphopoiesis (Mochizuki-Kashio et al., 2011; Muto et al., 2013). In the present study, we determined the individual and combinatory effects of *JAK2^V617F* and the loss of *Ezh2* on hematopoiesis.

　　PMF is a clonal hematopoietic disorder that is characterized by excessive fibrosis and impaired hematopoiesis ac-

companied by EMH. In the presence of *JAK2^V617F*, the loss of *Ezh2* caused progressive fibrosis accompanied by the expansion of dysplastic megakaryocytes in the BM and spleen, resulting in hypocellular BM and enhanced EMH in the spleen. The loss of *Ezh2* also promoted the output of mature myeloid cells but severely impaired erythropoiesis in part by enhancing apoptosis in erythroblasts. However, the JAK2^V617F/Ezh2^Δ/Δ mouse model differs from PMF patients in its milder to more modest fibrosis than that in PMF patients. Nevertheless, JAK2^V617F/Ezh2^Δ/Δ cells developed lethal MF with a markedly shorter latency than JAK2^V617F cells, and MF-initiating capacity was retained in the secondary recipients in a competitive setting. Because *EZH2* mutations independently predict poorer outcomes in patients with PMF (Guglielmelli et al., 2011), JAK2^V617F/Ezh2^Δ/Δ mice recapitulate the pheno-
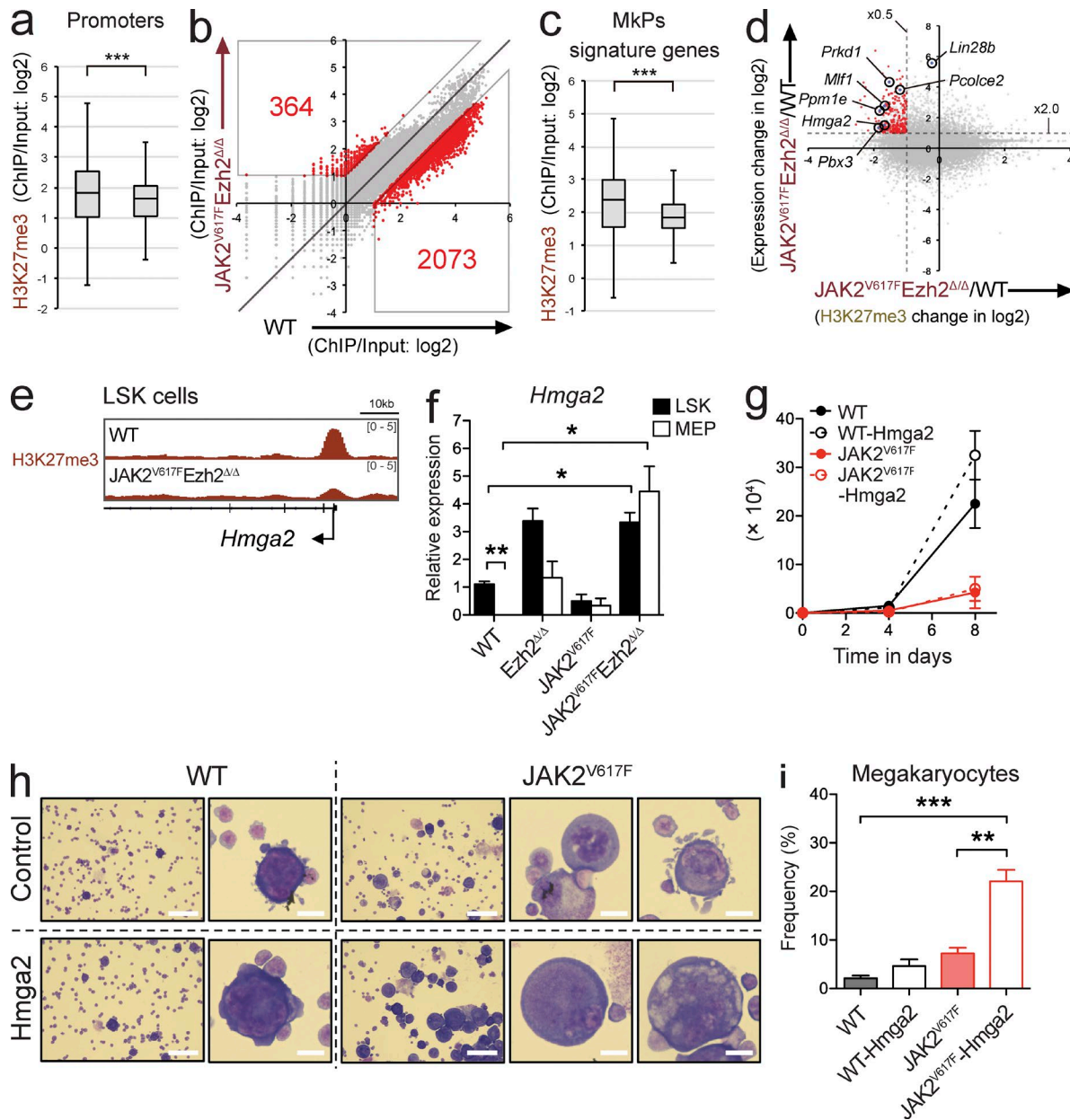
Figure 7. Alterations in H3K27me3 upon the loss of Ezh2 results in the activation of specific oncogenes. (a) Fold enrichment (ChIP/input) values of H3K27me3 (TSS ± 2.0 kb of RefSeq genes) in WT and JAK2^{V617F}/Ezh2$^{Δ/Δ}$ LSKs 4 wk after the deletion of *Ezh2*. (b) A scatter plot showing the relationship of fold enrichment (ChIP/input) values of H3K27me3 (TSS ± 2.0 kb of RefSeq genes) between WT and JAK2^{V617F}/Ezh2$^{Δ/Δ}$ LSKs 4 wk after the deletion of *Ezh2*. The light diagonal line represents the borderlines for twofold changes in H3K27me3 levels. (c) Fold enrichment (ChIP/input) values of H3K27me3 at TSS ± 2.0 kb of MkP signature genes in WT and JAK2^{V617F}/Ezh2$^{Δ/Δ}$ LSKs. (d) A scatter plot showing the relationship of expression of RefSeq genes in JAK2^{V617F}/Ezh2$^{Δ/Δ}$ LSKs relative to WT LSKs and H3K27me3 levels of RefSeq genes in JAK2^{V617F}/Ezh2$^{Δ/Δ}$ LSKs relative to WT LSKs and potential oncogenes activated in JAK2^{V617F}/Ezh2$^{Δ/Δ}$ LSKs (see also Table S2). (e) ChIP-seq view of H3K27me3 levels at the promoter region of *Hmga2* in WT and JAK2^{V617F}/Ezh2$^{Δ/Δ}$ LSKs 4 wk after the deletion of *Ezh2*. (f) qRT-PCR analysis of *Hmga2* in LSKs and MEPs from WT, Ezh2$^{Δ/Δ}$, JAK2^{V617F}, and JAK2^{V617F}/Ezh2$^{Δ/Δ}$ (*n* = 3–4) mice 1–2 mo after the deletion of *Ezh2*. (g) The total cell counts of WT (black lines) and JAK2^{V617F} (red lines) HSCs transduced with either a control (straight lines) or an *Hmga2* (broken lines) retrovirus were monitored for 8 d. (h) Representative pictures of *Hmga2*-transduced or control vector–transduced WT and JAK2^{V617F} HSCs on day 8 of the culture observed by May-Grünewald-Giemsa staining. Bars: 10 µm (high magnitude); 100 µm (low magnitude). (i) Proportions of megakaryocytes in *Hmga2*-transduced or control vector–transduced WT and JAK2^{V617F} HSCs on day 8 of the culture. (a and c) Boxes and whiskers show the mean and minimum to maximum, and asterisks show ***, P < 0.001 by the Student's *t* test; experiments used cells from two to four individual mice per genotype. (f, g, and i) Bars and asterisks show the mean ± SEM and *, P < 0.05; **, P < 0.01; and ***, P < 0.001 by the Student's *t* test; two independent experiments.
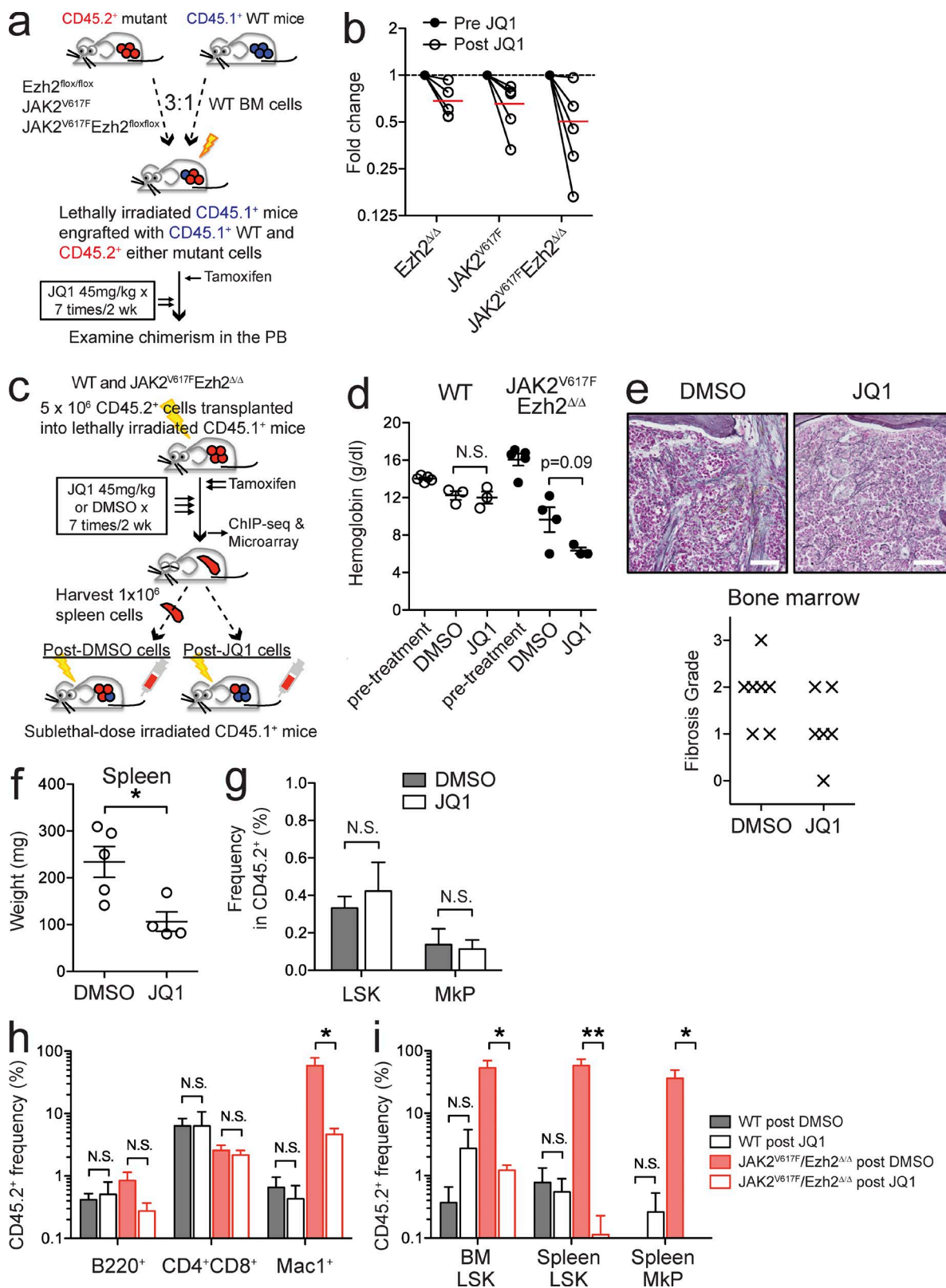
Figure 8. **Brd4 inhibition abrogates the MF–initiating capacity of JAK2^V617F/Ezh2^Δ/Δ cells.** (a) Experimental scheme of the JQ1 treatment of chimeric mice reconstituted with WT and mutant cells. (b) Fold changes in chimerism of CD45.2^+ mutant cells in Mac1^+ myeloid cells in the PB of recipients ($n = 5$ each) 8 wk after JQ1 administration compared with that of pre-JQ1 administration (red bars show the mean). (c) Experimental scheme of the JQ1 treatment

types of PMF patients better than $JAK2^{V617F}$ alone. A previous study reported that the acquisition of the $JAK2^{V617F}$ mutation alone was not sufficient for HSCs to initiate hematological malignancies in vivo (Mullally et al., 2010). We and another group demonstrated that additional mutations such as *TET2* mutations augmented the self-renewal capacity of $JAK2^{V617F}$ HSCs (Chen et al., 2015; Kameda et al., 2015). However, it is important to note that the order of the acquisition of *JAK2* and *TET2* mutations has been shown to affect clinical features, the biology of disease-initiating cells, and clonal evolution in patients with MPN (Ortmann et al., 2015). In the present study, we found that the down-regulated HSC signature in transcription in $JAK2^{V617F}$ mice was markedly attenuated by the loss of Ezh2. Together with the prominent effects of the loss of Ezh2 in $JAK2^{V617F}$–induced MF, our results suggested that loss-of-function mutations in *EZH2* augments the propagation capacity of $JAK2^{V617F}$ MF-initiating cells in patients, thereby promoting their clonal evolution in a manner similar to *TET2* mutations in $JAK2^{V617F}$ MPN.

We also noted that the majority of megakaryocytic genes were marked with H3K27me3 modifications by Ezh2 in LSK cells. However, MkP genes were positively enriched in $JAK2^{V617F}$/*Ezh2*-null LSKs only and not in *Ezh2*-null alone. These results indicated that $JAK2^{V617F}$ and the loss of Ezh2 cooperated to activate the differentiation program for megakaryopoiesis. Correspondingly, *Hmga2*, one of the PRC2 target genes de-repressed in the absence of Ezh2, markedly enhanced the megakaryocytic differentiation of HSCs in concert with $JAK2^{V617F}$ in cultures. This result is consistent with previous findings in which the overexpression of *Hmga2* induced MPN in mice lacking *Hmga2* 3′UTR or *Bmi1/Cdkn2a* double KO mice (Ikeda et al., 2011; Oguro et al., 2012), thereby strongly supporting the importance of *HMGA2* in the pathogenesis of PMF in patients harboring *EZH2* mutations.

BM fibrosis observed in PMF is reactive and mediated by various inflammatory cytokines such as TGF-β at pathogenic cellular and extracellular levels (Tefferi, 2005; Tefferi et al., 2011). Megakaryocytes and activated monocytes/neutrophils have been identified as a source of cytokines facilitating the formation of fibrosis, osteosclerosis, and angiogenesis in mouse models (Chagraoui et al., 2002; Zingariello et al., 2013). Although the pan-hematopoietic deletion of *Ezh2* led to the rapid progression of MF accompanied by the marked expansion of dysplastic megakaryocytes in $JAK2^{V617F}$ mice, the megakaryocyte-restricted deletion of *Ezh2* had a mild impact on the progression of MF and expansion of dysplastic mega-

karyocytes in $JAK2^{V617F}$ mice. Given that $JAK2^{V617F}$/$Ezh2^{\Delta/\Delta}$ mice also exhibited the expansion of myeloid cells, our results suggested the importance of functional cross-talk between megakaryocytes and myeloid cells in the pathogenesis of MF. The loss of Ezh2 may have an impact not only on megakaryocytes, but also on myeloid cells in this process. Further studies are needed to determine whether the pathogenic role of myeloid cells in the setting of the loss of Ezh2 is critical.

The loss of PRC2 has been shown to promote the consequential gain of H3K27ac, a transcriptional activating signal that recruits bromodomain–containing reader proteins (e.g., BRD4), in some settings (Pasini et al., 2010). A previous study demonstrated that the expression of SUZ12 increased H3K27me3 and decreased H3K27Ac in MPNST cells lacking SUZ12, whereas its ablation decreased H3K27me3 and increased H3K27Ac (De Raedt et al., 2014). BRD4 is a critical mediator of the positive transcriptional elongation complex of P-TEFb (Jang et al., 2005; Yang et al., 2005). BRD4 has been shown to recruit P-TEFb to promote the cell cycle transition (Yang et al., 2008) and activate c-Myc transcription (Rahl et al., 2010; Delmore et al., 2011), resulting in enhanced proliferation. In the present study, we also observed a mild increase in global H3K27ac levels in the setting of the loss of Ezh2. Importantly, $JAK2^{V617F}$/$Ezh2^{\Delta/\Delta}$ cells appeared to be more sensitive to JQ1, a bromodomain inhibitor (Filippakopoulos et al., 2010), and JQ1 profoundly compromised the MF-initiating capacity. A broad range of gene promoters showed a significant reduction in H3K27ac levels in JQ1-treated LK cells including the majority of PRC2 target genes. As a consequence, the expression of PRC2 targets as well as MkP genes was significantly down-regulated in JQ1-treated LSKs and MEPs. With the loss of Ezh2, the balance between H3K27me3 and H3K27ac modifications markedly changed at the promoter regions of PRC2 target genes, resulting in the de-repression of a list of PRC2 target genes including oncogenes such as *Hmga2*, whereas tumor suppressive PRC2 target genes were kept transcriptionally repressed or minimally transcribed. Once tumor-initiating cells adapt themselves to such conditions, they may become addicted to de-repressed oncogenic PRC2 target genes, thereby conferring sensitivity to bromodomain inhibition; however, it remains unknown how Brd4 inhibition reduced the levels of H3K27ac at promoter regions in $JAK2^{V617F}$/$Ezh2^{\Delta/\Delta}$ cells. BRD4 inhibition has been shown to abrogate AML cells harboring MLL-fusions in vivo, at least in part, by inhibiting critical oncogenes such as *c-Myc* (Dawson et al., 2011; Zuber et al., 2011). How-

---

of WT mice and $JAK2^{V617F}$/$Ezh2^{\Delta/\Delta}$ mice. (d) Hemoglobin levels of WT (open circles) and $JAK2^{V617F}$/$Ezh2^{\Delta/\Delta}$ (closed circles) mice pretreatment and 7 d after the completion of the JQ1 treatment. (e) Histology and fibrosis grading (grade 0–3) of the BM from DMSO-treated ($n = 7$) and JQ1-treated ($n = 6$) $JAK2^{V617F}$/$Ezh2^{\Delta/\Delta}$ mice observed by silver staining. Bars, 50 µm. (f) Spleen weight of DMSO-treated ($n = 5$) or JQ1-treated ($n = 4$) $JAK2^{V617F}$/$Ezh2^{\Delta/\Delta}$ mice 4 wk after the end of the treatment. (g) Proportions of LSKs and MkPs in the spleen of DMSO-treated and JQ1-treated $JAK2^{V617F}$/$Ezh2^{\Delta/\Delta}$ mice 4 wk after the completion of the treatment. (h and i) Chimerism of CD45.2^{+} cells in the PB (h) and BM LSKs, spleen LSKs, and spleen MkPs (i) of CD45.1[+] recipients ($n = 5$ each) at 4 mo after transplantation of 10^6 spleen cells isolated from DMSO-treated or JQ1-treated WT and $JAK2^{V617F}$/$Ezh2^{\Delta/\Delta}$ mice. (d and f–i) Bars and asterisks show the mean ± SEM and *, $P < 0.05$ by the Student's *t* test (d and f–h) or *, $P < 0.05$ and **, $P < 0.01$ by the Mann–Whitney *U* test (i); two independent experiments.
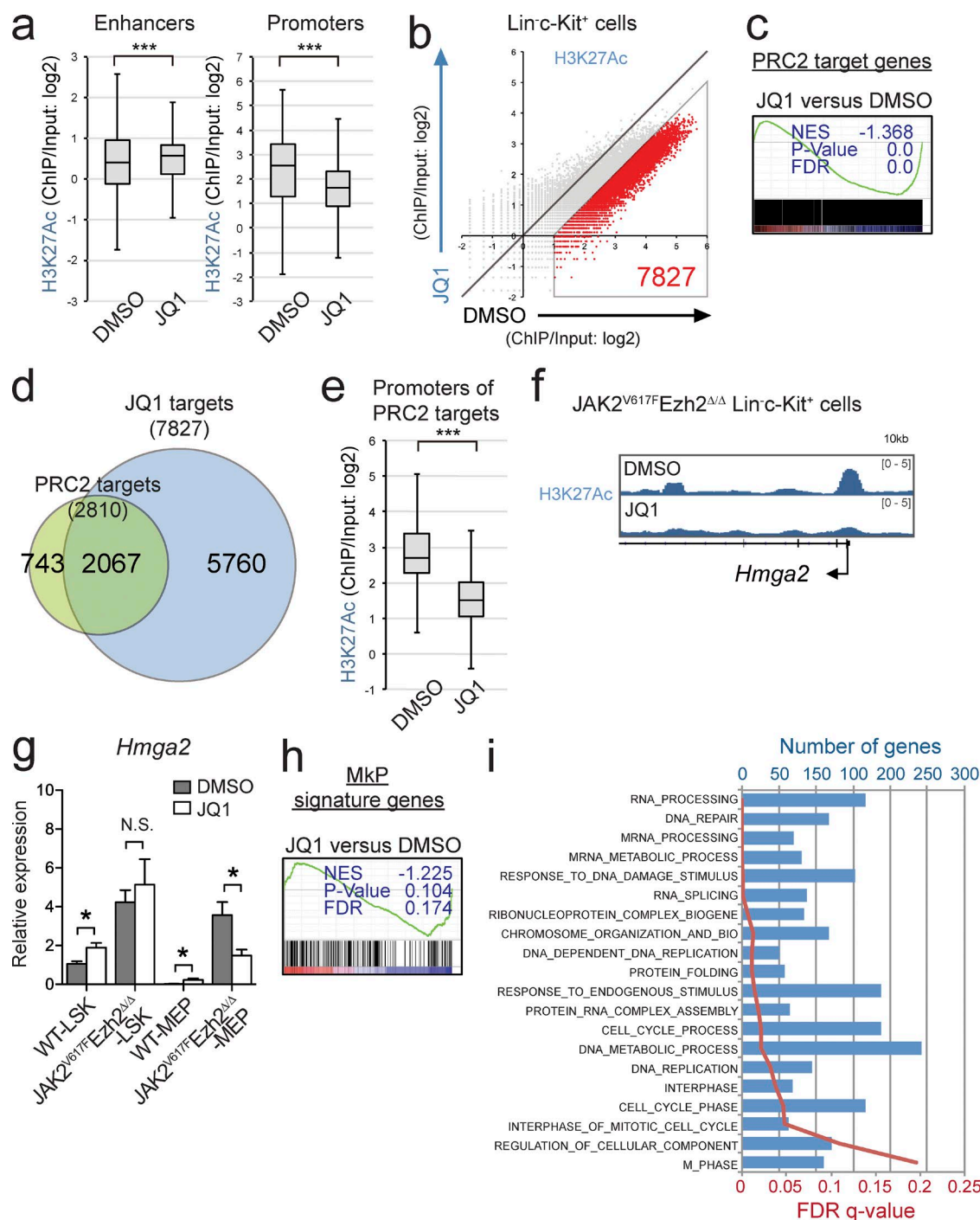
Figure 9. Brd4 inhibition restores de–repression of PRC2 target genes. (a) Fold enrichment (ChIP/input) values of H3K27ac at the enhancer and the promoter regions in JAK2^{V617F}/Ezh2$^{\Delta/\Delta}$ LK cells 2 wk after the completion of the JQ1 treatment. (b) A scatter plot showing the relationship of fold enrichment (ChIP/input) values of H3K27ac (TSS ± 2.0 kb of RefSeq genes) between DMSO- and JQ1-treated JAK2^{V617F}/Ezh2$^{\Delta/\Delta}$ LK cells (the light diagonal line represents the borderlines for twofold changes in H3K27ac levels). (c) GSEA plot for the canonical PRC2 targets defined in Fig. 7 b comparing LSKs in JQ1-treated with DMSO-treated JAK2^{V617F}/Ezh2$^{\Delta/\Delta}$ mice. (d) Venn diagrams showing overlaps between PRC2 target genes and JQ1 target genes, which were defined in b and are shown in Table S1. (e) Fold enrichment (ChIP/input) values of H3K27ac at the promoter regions of the canonical PRC2 target genes (defined in Fig. 7 b) in JAK2^{V617F}/Ezh2$^{\Delta/\Delta}$ LK cells 2 wk after the completion of the JQ1 treatment. (f) ChIP-seq view of H3K27ac levels at the promoter region of *Hmga2* in JQ1-treated or nontreated JAK2^{V617F}/Ezh2$^{\Delta/\Delta}$ LK cells. (g) qRT-PCR analysis of the expression of *Hmga2* in LSKs and MEPs isolated from DMSO-treated or JQ1-treated WT mice (n = 3) and JAK2^{V617F}/Ezh2$^{\Delta/\Delta}$ mice (n = 3) 2 wk after the completion of the treatment. (h) GSEA plot for the MkPs signature genes described in Fig. 6 g comparing LSK cells from JQ1-treated and DMSO-treated JAK2^{V617F}/Ezh2$^{\Delta/\Delta}$ mice. (i) GO biological process gene sets that were enriched

ever, we did not find a significant reduction in the expression of c-Myc targets between JQ1- and DMSO-treated LSKs. This result also supports MF-initiating cells being addicted to de-repressed PRC2 target genes in JAK2^{V617F}/Ezh2$^{\Delta/\Delta}$ mice. Collectively, these results demonstrated that the loss of Ezh2 cooperated with an active JAK2 mutant in the pathogenesis of MF and sensitized MF-initiating cells to bromodomain inhibition. Although we did not show any human data supporting our findings in this study, a significant portion of the PMF patients harbor both mutations (Guglielmelli et al., 2011; Nangalia et al., 2013). Therefore, it is warranted to further examine how *JAK2* and *EZH2* mutations collaborate to promote the disease and validate the efficacy of the bromodomain inhibition in patients.

Our study provides a new rationale for the application of bromodomain inhibitors to PMF patients with inactivating mutations or deletions in PRC2. It will also be interesting to combine bromodomain inhibitors with agents targeting the JAK2–STAT signaling pathway in PMF patients. Further studies are needed to improve the poor outcomes of patients with PMF using these new agents.

MATERIALS AND METHODS
Mice and transplantation. All mice were in the C57BL/6 background. *Ezh2* conditional KO (*Ezh2$^{flox/flox}$*) mice (provided by H. Koseki, RIKEN Center for Integrative Medical Sciences, Yokohama, Japan) were previously described (Hirabayashi et al., 2009) and crossed with *Rosa26::Cre-ERT2* mice (Taconic) for conditional deletion. *JAK2^{V617F}* transgenic mice (provided by K. Shimoda) were previously described (Shide et al., 2008). *Pf4-Cre* mice were previously described (Tiedt et al., 2007) and purchased from The Jackson Laboratory. C57BL/6 mice congenic for the Ly5 locus (CD45.1) were purchased from Sankyo-Lab Service. All experiments using these mice were performed in accordance with our institutional guidelines for the use of laboratory animals and approved by the Review Board for Animal Experiments of Chiba University (approval ID: 26-131). A total of 3–5 × 10^6 harvested BM cells from *Cre-ERT2*, *Ezh2$^{flox/flox}$;Cre-ERT2*, *JAK2^{V617F};Cre-ERT2*, and *JAK2^{V617F};Ezh2$^{flox/flox}$;Cre-ERT2* mice were intravenously injected in 8.5-Gy– or 9-Gy–irradiated CD45.1$^+$ mice. 4 wk after transplantation, 1 mg tamoxifen was administered via an intraperitoneal injection for five consecutive days to completely delete *Ezh2* alleles.

Retroviral transduction. *pMYs-IRES-GFP* and *pMYs-Hmga2-IRES-GFP* vectors were previously described (Kitamura et al., 2003). Retrovirus infection into CD34$^-$LSK HSCs was performed as previously described (Sashida et

al., 2014). In brief, retrovirus-infected 50 HSCs were cultured in SF-O3 medium containing 50 ng/ml mouse SCF and 50 ng/ml human TPO.

Flow cytometry and antibodies. Flow cytometry and cell sorting were performed by using the following monoclonal antibodies: CD45.2 (104), CD45.1 (A20), Gr1 (RB6-8C5), CD11b/Mac1 (M1/70), Ter119, CD71 (R17217), CD127/IL-7Ro (A7R34), B220 (RA3-6B2), CD4 (L3T4), CD8α (53-6.7), CD117/c-Kit (2B8), Sca-1 (D7), CD34 (MEC14.7), and FcγRII-III (93). These antibodies were purchased from eBioscience or BioLegend. The lineage mixture solution contained biotin-conjugated anti-Gr1, Mac1, B220, CD4, CD8α, Ter119, and IL-7Rα antibodies. Apoptotic cells were stained with an anti–Annexin V–APC antibody (550474; BD) and propidium iodide followed by the staining of cell surface markers to discriminate CD71$^+$Ter119$^+$ cells. All flow cytometry analyses and cell sorting were performed on FACSAria II or FACSCanto II (BD).

Cytokine stimulation and intracellular phosphoprotein analysis. Freshly isolated BM cells were cultured in 0.5% bovine serum albumin/RPMI at 37°C for 1 h and were stimulated with mouse 10 ng/ml IL-3 for 10 min. To evaluate intracellular phospho-Stat5, cultured BM cells were fixed and permeabilized and then detected by anti-Stat5 (pY694)–Alexa Fluor 647 (612599; BD) antibody after staining cells with lineage mixture, streptavidin-APC-Cy7, Sca-1–PE, c-Kit–PE-Cy7, and CD45.2-FITC antibodies. All flow cytometry analyses were performed on FACSCanto II.

qRT–PCR. qRT-PCR was performed on a StepOnePlus Real-Time PCR System (Thermo Fisher Scientific) by using SYBR Premix Ex Taq II (Takara Bio Inc.) or FastStart Universal Probe Master (Roche) with a Universal Probe Library (Roche). Primer sequences (forward and reverse primers) and Universal ProbeLibrary (Roche) numbers are shown for *Ezh2* (5′-CCAGACTGGTGAAGAGTTGTTTT-3′/5′-CAAGGGATTTCCATTTCTCG-3′/#105), *Hmga2* (5′-AAGGCAGCAAAAACAAGAGC-3′/5′-GCCGTTTTTCTCCAATGGT-3′/#26), and *Gapdh* (5′-ATGACATCAAGAAGGTGGTGAAG-3′/5′-TCCTTGGAGGCCATGTAGG-3′). All data are presented as relative expression levels normalized to *Gapdh* expression.

Microarray analysis and data analysis. Total RNA was extracted from ∼2 × 10^5 pooled BM LSK cells (isolated from two to four mice per each genotype) using an RNeasy Plus Mini kit (QIAGEN). 20 ng of total RNA was mixed with

more in JQ-treated LSK cells than in DMSO-treated LSK cells as determined by GSEA (gene sizes and FDR q-values are shown in the top and bottom x axes). (a and e) Boxes and whiskers show the mean and minimum to maximum. The asterisks show ***, P < 0.001 by the Student's *t* test. (c, h, and i) The normalized enrichment score (NES), nominal p-value, and false discovery rate (FDR) q-value are indicated. (a–f, h, and i) Experiments used cells from two individual mice per group. (g) Bars and asterisks show the mean ± SEM and *, P < 0.05 by the Student's *t* test; two independent experiments.

spike–in controls using a One Color Spike Mix kit (Agilent Technologies), amplified, and labeled with Cyanine 3 using a Low Input Quick Amp Labeling kit (Agilent Technologies) according to the manufacturer's instructions. A microarray analysis using a SurePrint G3 Mouse GE Microarray 8 × 60K kit (Agilent Technologies) was performed according to the manufacturer's instructions. Raw data were deposited in Gene Expression Omnibus under the accession no. GSE69500. Hierarchical clustering and principal component analyses based on total gene expression were performed using MeV (Multiple Experiment Viewer) software.

Western blotting. Antibodies for Western blotting were as follows: anti-H3K27me3 (07449; EMD Millipore), anti-H3K27ac (ab4729; Abcam), anti-H3 (ab1791; Abcam), anti-Ezh2 (5246; CST), anti-Jak2 (3230; CST), and anti–β–Actin (sc–47778; Santa Cruz Biotechnology, Inc.). β–Actin and histone H3 were detected as loading controls.

ChIP–seq. ChIP assays were performed as previously described (Muto et al., 2013). In brief, 10^5 pooled BM LSK cells (isolated from two to four mice per each genotype) were used for each immunoprecipitation. The following antibodies were used for the immunoprecipitation reactions: anti–H3K27me3 (07449; EMD Millipore) and anti-H3K27ac (ab4729; Abcam). ChIP-seq data have been deposited in the NCBI BioProject database under accession no. PRJDB3992.

Sequencing data analysis. The ChIP-seq signal was quantified as the total number of reads per million. To evaluate the histone modification mark of each gene, normalized tag numbers in the region from 2 kb upstream to 2 kb downstream of the TSS were counted and divided by the tag number of the corresponding input. The RPKM (reads per kilobase of transcripts per million mapped reads) values of the sequenced reads were calculated every 5,000-bp bin with a shifting size of 500 bp using BEDTools to be visualized with the Integrative Genomics Viewer (IGV) genome browser. The read numbers of the immunoprecipitated samples were then normalized by subtracting the RPKM values of the input samples in each bin and converted to a bigwig file using the wigToBigWig tool. The super-computing resource was provided by the Human Genome Center, the Institute of Medical Science, the University of Tokyo (http://sc.hgc.jp/shirokane.html). Canonical PRC2 target genes were defined as those with fold enrichment of H3K27me3 ChIP signals greater than twofold over the input signals (ChIP/input) in WT LSK cells (Table S1).

Statistical analysis. The statistical significance of differences was measured by unpaired two-tailed Student's *t* test or Mann–Whitney nonparametric test. All statistical tests were performed using Prism version 5 (GraphPad Software). All experiments were conducted and confirmed at least two replicates.

Accession numbers. Microarray data have been deposited in the Gene Expression Omnibus database under the accession no. GSE69500. ChIP-seq data have been deposited in the NCBI BioProject database under accession no. PRJDB3992.

Online supplemental material. Table S1, included as an Excel file, lists canonical PRC2 target genes identified in LSK cells and JQ1 target genes identified in LK cells. Table S2, included as an Excel file, lists potential oncogenes highly expressed after reduction in H3K27me3 levels in JAK2^{V617F}/Ezh2$^{\Delta/\Delta}$ LSK cells. Online supplemental material is available at http://www.jem.org/cgi/content/full/jem.20151121/DC1.

REFERENCES

Baxter, E.J., L.M. Scott, P.J. Campbell, C. East, N. Fourouclas, S. Swanton, G.S. Vassiliou, A.J. Bench, E.M. Boyd, N. Curtin, et al. Cancer Genome Project. 2005. Acquired mutation of the tyrosine kinase JAK2 in human myeloproliferative disorders. *Lancet*. 365:1054–1061. http://dx.doi.org/10.1016/S0140-6736(05)74230-6

Béguelin, W., R. Popovic, M. Teater, Y. Jiang, K.L. Bunting, M. Rosen, H. Shen, S.N. Yang, L. Wang, T. Ezponda, et al. 2013. EZH2 is required for germinal center formation and somatic EZH2 mutations promote lymphoid transformation. *Cancer Cell*. 23:677–692. http://dx.doi.org/10.1016/j.ccr.2013.04.011

Bejar, R., K. Stevenson, O. Abdel-Wahab, N. Galili, B. Nilsson, G. Garcia-Manero, H. Kantarjian, A. Raza, R.L. Levine, D. Neuberg, and B.L. Ebert. 2011. Clinical effect of point mutations in myelodysplastic syndromes. *N. Engl. J. Med*. 364:2496–2506. http://dx.doi.org/10.1056/NEJMoa1013343

Cao, R., L. Wang, H. Wang, L. Xia, H. Erdjument-Bromage, P. Tempst, R.S. Jones, and Y. Zhang. 2002. Role of histone H3 lysine 27 methylation in Polycomb-group silencing. *Science*. 298:1039–1043. http://dx.doi.org/10.1126/science.1076997

Chagraoui, H., E. Komura, M. Tulliez, S. Giraudier, W. Vainchenker, and F. Wendling. 2002. Prominent role of TGF-β1 in thrombopoietin-induced myelofibrosis in mice. *Blood*. 100:3495–3503. http://dx.doi.org/10.1182/blood-2002-04-1133

Chambers, S.M., N.C. Boles, K.-Y.K. Lin, M.P. Tierney, T.V. Bowman, S.B. Bradfute, A.J. Chen, A.A. Merchant, O. Sirin, D.C. Weksberg, et al. 2007. Hematopoietic fingerprints: an expression database of stem cells and

their progeny. *Cell Stem Cell.* 1:578–591. http://dx.doi.org/10.1016/j.stem.2007.10.003

Chen, E., R.K. Schneider, L.J. Breyfogle, E.A. Rosen, L. Poveromo, S. Elf, A. Ko, K. Brumme, R. Levine, B.L. Ebert, and A. Mullally. 2015. Distinct effects of concomitant Jak2V617F expression and Tet2 loss in mice promote disease progression in myeloproliferative neoplasms. *Blood.* 125:327–335. http://dx.doi.org/10.1182/blood-2014-04-567024

Dawson, M.A., R.K. Prinjha, A. Dittmann, G. Giotopoulos, M. Bantscheff, W.I. Chan, S.C. Robson, C.W. Chung, C. Hopf, M.M. Savitski, et al. 2011. Inhibition of BET recruitment to chromatin as an effective treatment for MLL-fusion leukaemia. *Nature.* 478:529–533. http://dx.doi.org/10.1038/nature10509

Delmore, J.E., G.C. Issa, M.E. Lemieux, P.B. Rahl, J. Shi, H.M. Jacobs, E. Kastritis, T. Gilpatrick, R.M. Paranal, J. Qi, et al. 2011. BET bromodomain inhibition as a therapeutic strategy to target c-Myc. *Cell.* 146:904–917. http://dx.doi.org/10.1016/j.cell.2011.08.017

De Raedt, T., E. Beert, E. Pasmant, A. Luscan, H. Brems, N. Ortonne, K. Helin, J.L. Hornick, V. Mautner, H. Kehrer-Sawatzki, et al. 2014. PRC2 loss amplifies Ras-driven transcription and confers sensitivity to BRD4-based therapies. *Nature.* 514:247–251. http://dx.doi.org/10.1038/nature13561

Filippakopoulos, P., J. Qi, S. Picaud, Y. Shen, W.B. Smith, O. Fedorov, E.M. Morse, T. Keates, T.T. Hickman, I. Felletar, et al. 2010. Selective inhibition of BET bromodomains. *Nature.* 468:1067–1073. http://dx.doi.org/10.1038/nature09504

Guglielmelli, P., R. Zini, C. Bogani, S. Salati, A. Pancrazzi, E. Bianchi, F. Mannelli, S. Ferrari, M.-C. Le Bousse-Kerdilès, A. Bosi, et al. 2007. Molecular profiling of CD34$^+$ cells in idiopathic myelofibrosis identifies a set of disease-associated genes and reveals the clinical significance of Wilms' tumor gene 1 (*WT1*). *Stem Cells.* 25:165–173. http://dx.doi.org/10.1634/stemcells.2006-0351

Guglielmelli, P., F. Biamonte, J. Score, C. Hidalgo-Curtis, F. Cervantes, M. Maffioli, T. Fanelli, T. Ernst, N. Winkelman, A.V. Jones, et al. 2011. EZH2 mutational status predicts poor survival in myelofibrosis. *Blood.* 118:5227–5234. http://dx.doi.org/10.1182/blood-2011-06-363424

Haas, S., J. Hansson, D. Klimmeck, D. Loeffler, L. Velten, H. Uckelmann, S. Wurzer, Á.M. Prendergast, A. Schnell, K. Hexel, et al. 2015. Inflammation-induced emergency megakaryopoiesis driven by hematopoietic stem cell-like megakaryocyte progenitors. *Cell Stem Cell.* 17:422–434. http://dx.doi.org/10.1016/j.stem.2015.07.007

Harada-Shirado, K., K. Ikeda, K. Ogawa, H. Ohkawara, H. Kimura, T. Kai, H. Noji, S. Morishita, N. Komatsu, and Y. Takeishi. 2015. Dysregulation of the MIRLET7/HMGA2 axis with methylation of the CDKN2A promoter in myeloproliferative neoplasms. *Br. J. Haematol.* 168:338–349. http://dx.doi.org/10.1111/bjh.13129

Herrera-Merchan, A., L. Arranz, J.M. Ligos, A. de Molina, O. Dominguez, and S. Gonzalez. 2012. Ectopic expression of the histone methyltransferase Ezh2 in haematopoietic stem cells causes myeloproliferative disease. *Nat. Commun.* 3:623. http://dx.doi.org/10.1038/ncomms1623

Hirabayashi, Y., N. Suzki, M. Tsuboi, T.A. Endo, T. Toyoda, J. Shinga, H. Koseki, M. Vidal, and Y. Gotoh. 2009. Polycomb limits the neurogenic competence of neural precursor cells to promote astrogenic fate transition. *Neuron.* 63:600–613. http://dx.doi.org/10.1016/j.neuron.2009.08.021

Ikeda, K., P.J. Mason, and M. Bessler. 2011. 3′UTR-truncated Hmga2 cDNA causes MPN-like hematopoiesis by conferring a clonal growth advantage at the level of HSC in mice. *Blood.* 117:5860–5869. http://dx.doi.org/10.1182/blood-2011-02-334425

Jang, M.K., K. Mochizuki, M. Zhou, H.S. Jeong, J.N. Brady, and K. Ozato. 2005. The bromodomain protein Brd4 is a positive regulatory component of P-TEFb and stimulates RNA polymerase II-dependent transcription. *Mol. Cell.* 19:523–534. http://dx.doi.org/10.1016/j.molcel.2005.06.027

Kakumitsu, H., K. Kamezaki, K. Shimoda, K. Karube, T. Haro, A. Numata, K. Shide, T. Matsuda, K. Oshima, and M. Harada. 2005. Transgenic mice overexpressing murine thrombopoietin develop myelofibrosis and osteosclerosis. *Leuk. Res.* 29:761–769. http://dx.doi.org/10.1016/j.leukres.2004.12.009

Kameda, T., K. Shide, T. Yamaji, A. Kamiunten, M. Sekine, Y. Taniguchi, T. Hidaka, Y. Kubuki, H. Shimoda, K. Marutsuka, et al. 2015. Loss of TET2 has dual roles in murine myeloproliferative neoplasms: disease sustainer and disease accelerator. *Blood.* 125:304–315. http://dx.doi.org/10.1182/blood-2014-04-555508

Kitamura, T., Y. Koshino, F. Shibata, T. Oki, H. Nakajima, T. Nosaka, and H. Kumagai. 2003. Retrovirus-mediated gene transfer and expression cloning: powerful tools in functional genomics. *Exp. Hematol.* 31:1007–1014. http://dx.doi.org/10.1016/S0301-472X(03)00260-1

Klampfl, T., H. Gisslinger, A.S. Harutyunyan, H. Nivarthi, E. Rumi, J.D. Milosevic, N.C.C. Them, T. Berg, B. Gisslinger, D. Pietra, et al. 2013. Somatic mutations of calreticulin in myeloproliferative neoplasms. *N. Engl. J. Med.* 369:2379–2390. http://dx.doi.org/10.1056/NEJMoa1311347

Kotini, A.G., C.J. Chang, I. Boussaad, J.J. Delrow, E.K. Dolezal, A.B. Nagulapally, F. Perna, G.A. Fishbein, V.M. Klimek, R.D. Hawkins, et al. 2015. Functional analysis of a chromosomal deletion associated with myelodysplastic syndromes using isogenic human induced pluripotent stem cells. *Nat. Biotechnol.* 33:646–655. http://dx.doi.org/10.1038/nbt.3178

Kralovics, R., F. Passamonti, A.S. Buser, S.S. Teo, R. Tiedt, J.R. Passweg, A. Tichelli, M. Cazzola, and R.C. Skoda. 2005. A gain-of-function mutation of JAK2 in myeloproliferative disorders. *N. Engl. J. Med.* 352:1779–1790. http://dx.doi.org/10.1056/NEJMoa051113

Lara-Astiaso, D., A. Weiner, E. Lorenzo-Vivas, I. Zaretsky, D.A. Jaitin, E. David, H. Keren-Shaul, A. Mildner, D. Winter, S. Jung, et al. 2014. Chromatin state dynamics during blood formation. *Science.* 345:943–949. http://dx.doi.org/10.1126/science.1256271

Levine, R.L., A. Pardanani, A. Tefferi, and D.G. Gilliland. 2007. Role of JAK2 in the pathogenesis and therapy of myeloproliferative disorders. *Nat. Rev. Cancer.* 7:673–683. http://dx.doi.org/10.1038/nrc2210

Lundberg, P., H. Takizawa, L. Kubovcakova, G. Guo, H. Hao-Shen, S. Dirnhofer, S.H. Orkin, M.G. Manz, and R.C. Skoda. 2014. Myeloproliferative neoplasms can be initiated from a single hematopoietic stem cell expressing JAK2-V617F. *J. Exp. Med.* 211:2213–2230. http://dx.doi.org/10.1084/jem.20131371

Mochizuki-Kashio, M., Y. Mishima, S. Miyagi, M. Negishi, A. Saraya, T. Konuma, J. Shinga, H. Koseki, and A. Iwama. 2011. Dependency on the polycomb gene Ezh2 distinguishes fetal from adult hematopoietic stem cells. *Blood.* 118:6553–6561. http://dx.doi.org/10.1182/blood-2011-03-340554

Morin, R.D., N.A. Johnson, T.M. Severson, A.J. Mungall, J. An, R. Goya, J.E. Paul, M. Boyle, B.W. Woolcock, F. Kuchenbauer, et al. 2010. Somatic mutations altering EZH2 (Tyr641) in follicular and diffuse large B-cell lymphomas of germinal-center origin. *Nat. Genet.* 42:181–185. http://dx.doi.org/10.1038/ng.518

Mullally, A., S.W. Lane, B. Ball, C. Megerdichian, R. Okabe, F. Al-Shahrour, M. Paktinat, J.E. Haydu, E. Housman, A.M. Lord, et al. 2010. Physiological Jak2V617F expression causes a lethal myeloproliferative neoplasm with differential effects on hematopoietic stem and progenitor cells. *Cancer Cell.* 17:584–596. http://dx.doi.org/10.1016/j.ccr.2010.05.015

Muto, T., G. Sashida, M. Oshima, G.R. Wendt, M. Mochizuki-Kashio, Y. Nagata, M. Sanada, S. Miyagi, A. Saraya, A. Kamio, et al. 2013. Concurrent loss of Ezh2 and Tet2 cooperates in the pathogenesis of myelodysplastic disorders. *J. Exp. Med.* 210:2627–2639. http://dx.doi.org/10.1084/jem.20131144

Nangalia, J., C.E. Massie, E.J. Baxter, F.L. Nice, G. Gundem, D.C. Wedge, E. Avezov, J. Li, K. Kollmann, D.G. Kent, et al. 2013. Somatic CALR mutations

in myeloproliferative neoplasms with nonmutated JAK2. *N. Engl. J. Med.* 369:2391–2405. http://dx.doi.org/10.1056/NEJMoa1312542

Neff, T., A.U. Sinha, M.J. Kluk, N. Zhu, M.H. Khattab, L. Stein, H. Xie, S.H. Orkin, and S.A. Armstrong. 2012. Polycomb repressive complex 2 is required for MLL-AF9 leukemia. *Proc. Natl. Acad. Sci. USA.* 109:5028–5033. http://dx.doi.org/10.1073/pnas.1202258109

Oguro, H., J. Yuan, S. Tanaka, S. Miyagi, M. Mochizuki-Kashio, H. Ichikawa, S. Yamazaki, H. Koseki, H. Nakauchi, and A. Iwama. 2012. Lethal myelofibrosis induced by Bmi1-deficient hematopoietic cells unveils a tumor suppressor function of the polycomb group genes. *J. Exp. Med.* 209:445–454. http://dx.doi.org/10.1084/jem.20111709

Ortmann, C.A., D.G. Kent, J. Nangalia, Y. Silber, D.C. Wedge, J. Grinfeld, E.J. Baxter, C.E. Massie, E. Papaemmanuil, S. Menon, et al. 2015. Effect of mutation order on myeloproliferative neoplasms. *N. Engl. J. Med.* 372:601–612. http://dx.doi.org/10.1056/NEJMoa1412098

Pasini, D., M. Malatesta, H.R. Jung, J. Walfridsson, A. Willer, L. Olsson, J. Skotte, A. Wutz, B. Porse, O.N. Jensen, and K. Helin. 2010. Characterization of an antagonistic switch between histone H3 lysine 27 methylation and acetylation in the transcriptional regulation of Polycomb group target genes. *Nucleic Acids Res.* 38:4958–4969. http://dx.doi.org/10.1093/nar/gkq244

Pronk, C.J.H., D.J. Rossi, R. Månsson, J.L. Attema, G.L. Norddahl, C.K.F. Chan, M. Sigvardsson, I.L. Weissman, and D. Bryder. 2007. Elucidation of the phenotypic, functional, and molecular topography of a myeloerythroid progenitor cell hierarchy. *Cell Stem Cell.* 1:428–442. http://dx.doi.org/10.1016/j.stem.2007.07.005

Rahl, P.B., C.Y. Lin, A.C. Seila, R.A. Flynn, S. McCuine, C.B. Burge, P.A. Sharp, and R.A. Young. 2010. c-Myc regulates transcriptional pause release. *Cell.* 141:432–445. http://dx.doi.org/10.1016/j.cell.2010.03.030

Sashida, G., and A. Iwama. 2012. Epigenetic regulation of hematopoiesis. *Int. J. Hematol.* 96:405–412. http://dx.doi.org/10.1007/s12185-012-1183-x

Sashida, G., H. Harada, H. Matsui, M. Oshima, M. Yui, Y. Harada, S. Tanaka, M. Mochizuki-Kashio, C. Wang, A. Saraya, et al. 2014. Ezh2 loss promotes development of myelodysplastic syndrome but attenuates its predisposition to leukaemic transformation. *Nat. Commun.* 5:4177. http://dx.doi.org/10.1038/ncomms5177

Sauvageau, M., and G. Sauvageau. 2010. Polycomb group proteins: multi-faceted regulators of somatic stem cells and cancer. *Cell Stem Cell.* 7:299–313. http://dx.doi.org/10.1016/j.stem.2010.08.002

Shide, K., H.K. Shimoda, T. Kumano, K. Karube, T. Kameda, K. Takenaka, S. Oku, H. Abe, K.S. Katayose, Y. Kubuki, et al. 2008. Development of ET, primary myelofibrosis and PV in mice expressing JAK2V617F. *Leukemia.* 22:87–95. http://dx.doi.org/10.1038/sj.leu.2405043

Shih, A.H., O. Abdel-Wahab, J.P. Patel, and R.L. Levine. 2012. The role of mutations in epigenetic regulators in myeloid malignancies. *Nat. Rev. Cancer.* 12:599–612. http://dx.doi.org/10.1038/nrc3343

Subramanian, A., P. Tamayo, V.K. Mootha, S. Mukherjee, B.L. Ebert, M.A. Gillette, A. Paulovich, S.L. Pomeroy, T.R. Golub, E.S. Lander, and J.P. Mesirov. 2005. Gene set enrichment analysis: a knowledge-based approach for interpreting genome-wide expression profiles. *Proc. Natl.*

Acad. Sci. USA. 102:15545–15550. http://dx.doi.org/10.1073/pnas.0506580102

Tanaka, S., S. Miyagi, G. Sashida, T. Chiba, J. Yuan, M. Mochizuki-Kashio, Y. Suzuki, S. Sugano, C. Nakaseko, K. Yokote, et al. 2012. Ezh2 augments leukemogenicity by reinforcing differentiation blockage in acute myeloid leukemia. *Blood.* 120:1107–1117. http://dx.doi.org/10.1182/blood-2011-11-394932

Tefferi, A. 2005. Pathogenesis of myelofibrosis with myeloid metaplasia. *J. Clin. Oncol.* 23:8520–8530. http://dx.doi.org/10.1200/JCO.2004.00.9316

Tefferi, A., R. Vaidya, D. Caramazza, C. Finke, T. Lasho, and A. Pardanani. 2011. Circulating interleukin (IL)-8, IL-2R, IL-12, and IL-15 levels are independently prognostic in primary myelofibrosis: a comprehensive cytokine profiling study. *J. Clin. Oncol.* 29:1356–1363. http://dx.doi.org/10.1200/JCO.2010.32.9490

Thiele, J., H.M. Kvasnicka, F. Facchetti, V. Franco, J. van der Walt, and A. Orazi. 2005. European consensus on grading bone marrow fibrosis and assessment of cellularity. *Haematologica.* 90:1128–1132.

Tiedt, R., T. Schomber, H. Hao-Shen, and R.C. Skoda. 2007. Pf4-Cre transgenic mice allow the generation of lineage-restricted gene knockouts for studying megakaryocyte and platelet function in vivo. *Blood.* 109:1503–1506. http://dx.doi.org/10.1182/blood-2006-04-020362

Wang, X., S. Prakash, M. Lu, J. Tripodi, F. Ye, V. Najfeld, Y. Li, M. Schwartz, R. Weinberg, P. Roda, et al. 2012. Spleens of myelofibrosis patients contain malignant hematopoietic stem cells. *J. Clin. Invest.* 122:3888–3899. http://dx.doi.org/10.1172/JCI64397

Xie, H., J. Xu, J.H. Hsu, M. Nguyen, Y. Fujiwara, C. Peng, and S.H. Orkin. 2014. Polycomb repressive complex 2 regulates normal hematopoietic stem cell function in a developmental-stage-specific manner. *Cell Stem Cell.* 14:68–80. http://dx.doi.org/10.1016/j.stem.2013.10.001

Yamamoto, R., Y. Morita, J. Ooehara, S. Hamanaka, M. Onodera, K.L. Rudolph, H. Ema, and H. Nakauchi. 2013. Clonal analysis unveils self-renewing lineage-restricted progenitors generated directly from hematopoietic stem cells. *Cell.* 154:1112–1126. http://dx.doi.org/10.1016/j.cell.2013.08.007

Yang, Z., J.H.N. Yik, R. Chen, N. He, M.K. Jang, K. Ozato, and Q. Zhou. 2005. Recruitment of P-TEFb for stimulation of transcriptional elongation by the bromodomain protein Brd4. *Mol. Cell.* 19:535–545. http://dx.doi.org/10.1016/j.molcel.2005.06.029

Yang, Z., N. He, and Q. Zhou. 2008. Brd4 recruits P-TEFb to chromosomes at late mitosis to promote G1 gene expression and cell cycle progression. *Mol. Cell. Biol.* 28:967–976. http://dx.doi.org/10.1128/MCB.01020-07

Zingariello, M., F. Martelli, F. Ciaffoni, F. Masiello, B. Ghinassi, E.D. Amore, M. Massa, G. Barosi, L. Sancillo, X. Li, et al. 2013. Characterization of the TGF-β1 signaling abnormalities in the Gata1low mouse model of myelofibrosis. *Blood.* 121:3345–3363. http://dx.doi.org/10.1182/blood-2012-06-439661

Zuber, J., J. Shi, E. Wang, A.R. Rappaport, H. Herrmann, E.A. Sison, D. Magoon, J. Qi, K. Blatt, M. Wunderlich, et al. 2011. RNAi screen identifies Brd4 as a therapeutic target in acute myeloid leukaemia. *Nature.* 478:524–528. http://dx.doi.org/10.1038/nature10334